AWARD NUMBER: W81XWH-13-1-0482

TITLE: Treatment of Neuropathic Pain after SCI with a Catalytic Oxidoreductant

PRINCIPAL INVESTIGATOR: Candace L. Floyd, Ph.D.

CONTRACTING ORGANIZATION:
University of Alabama at Birmingham
Birmingham AL, 35249-7330

REPORT DATE:
October 2015

TYPE OF REPORT:
Annual

PREPARED FOR: U.S. Army Medical Research and Materiel Command
                Fort Detrick, Maryland 21702-5012

DISTRIBUTION STATEMENT: Approved for Public Release;
                        Distribution Unlimited

REPORT DOCUMENTATION PAGE

Form Approved
OMB No. 0704-0188

Public reporting burden for this collection of information is estimated to average 1 hour per response, including the time for reviewing instructions, searching existing data sources, gathering and maintaining the data needed, and completing and reviewing this collection of information. Send comments regarding this burden estimate or any other aspect of this collection of information, including suggestions for reducing this burden to Department of Defense, Washington Headquarters Services, Directorate for Information Operations and Reports (0704-0188), 1215 Jefferson Davis Highway, Suite 1204, Arlington, VA 22202-4302. Respondents should be aware that notwithstanding any other provision of law, no person shall be subject to any penalty for failing to comply with a collection of information if it does not display a currently valid OMB control number. **PLEASE DO NOT RETURN YOUR FORM TO THE ABOVE ADDRESS.**

1. REPORT DATE	2. REPORT TYPE	3. DATES COVERED
October 2015	Annual	30 Sep 2014 - 29 Sep 2015

4. TITLE AND SUBTITLE

Treatment of Neuropathic Pain after SCI with a Catalytic Oxidoreductant

5a. CONTRACT NUMBER

5b. GRANT NUMBER
W81XWH-13-1-0482

5c. PROGRAM ELEMENT NUMBER

6. AUTHOR(S)
Candace L. Floyd, Ph.D.

E-Mail:clfloyd@uab.edu

5d. PROJECT NUMBER

5e. TASK NUMBER

5f. WORK UNIT NUMBER

7. PERFORMING ORGANIZATION NAME(S) AND ADDRESS(ES)
University of Alabama at Birmingham
Spain Rehabilitation Center Room 529
1717 6th Avenue South
Birmingham AL, 35249-7330

8. PERFORMING ORGANIZATION REPORT NUMBER

9. SPONSORING / MONITORING AGENCY NAME(S) AND ADDRESS(ES)

U.S. Army Medical Research and Materiel Command

Fort Detrick, Maryland 21702-5012

10. SPONSOR/MONITOR'S ACRONYM(S)

11. SPONSOR/MONITOR'S REPORT NUMBER(S)

12. DISTRIBUTION / AVAILABILITY STATEMENT

Approved for Public Release; Distribution Unlimited

13. SUPPLEMENTARY NOTES

14. ABSTRACT
The on-going research is to test the central hypothesis that post-SCI administration of the catalytic oxidoreductant BuOE will inhibit neuropathic pain after SCI. The research in years 1 and 2 focused on the goal of aims 1 and 2, to test the hypothesis that post-SCI administration of BuOE decreases inflammation and ROS activation in a rat and mouse model of SCI. The main finding of our work in this year was to evaluate the dose-effect curve of post-SCI administration of BuOE on the outcomes listed above. Our data from on-going experiments indicate that the dose of 0.2mg/kg BuOE was most effective in reducing inflammation and ROS activation acutely post-SCI in rats and mice. On-going experiments will evaluate additional outcome measures and behavioral outcomes in the subsequent year.

15. SUBJECT TERMS

16. SECURITY CLASSIFICATION OF:

a. REPORT	b. ABSTRACT	c. THIS PAGE	17. LIMITATION OF ABSTRACT	18. NUMBER OF PAGES	19a. NAME OF RESPONSIBLE PERSON USAMRMC
Unclassified	Unclassified	Unclassified	Unclassified		19b. TELEPHONE NUMBER (include area code)

Standard Form 298 (Rev. 8-98)
Prescribed by ANSI Std. Z39.18

Table of Contents

1. INTRODUCTION:

Although the neurobiological mechanisms that underlie neuropathic pain are poorly understood, we hypothesize that a highly efficacious treatment for neuropathic pain after SCI would be a molecule that scavenges ROS, inhibits NF-κB activation, is bioavailable to the CNS, and is well tolerated. We have extensive experience in the development of a class of therapeutic catalytic oxidoreductants which *both* dissipate ROS *and* inhibit NF-κB activation. Thus, the objective of this research is to evaluate MnTnBuOE-2-PyP^{5+} (BuOE2) as a novel therapeutic to treat neuropathic pain after SCI as it offers the unique and simultaneous chemistry of direct redox-regulation of pro-inflammatory promoting signaling pathways and dissipation of ROS. The proposed research will test the central hypothesis that post-SCI administration of the catalytic oxidoreductant BuOE2 will inhibit neuropathic pain after SCI by assessing the effects of post-SCI administration of BuOE2 on ROS, NF-κB signaling, inflammation, and pain-associated behaviors in a clinically relevant *rat* model of *cervical contusion* SCI and a *mouse* model of *ischemic* SCI (Aims 1 and 2). The experiments of efficacy in rodent models will then be followed up in a large animal model of SCI, the porcine contusion model (Aim 3).

2. KEY WORDS:

Neuropathic pain, spinal cord injury, reactive oxygen species, cervical contusion, ischemic spinal cord injury, oxidative stress, inflammation

3. ACCOMPLISHMENTS

Major Goals of the Project in Years 1 and 2:

The years 1 and 2 major goals/ deliverables were to:

- **Perform pharmacokinetic analysis of subcutaneous BuOE2 in both rats and mice**
  We have successfully completed this goal and determined the PK for administration of BuOE2 in rats in mice. Parts of these data are included in the manuscript by Tovmasyan et al, submitted to ReDox Biology (appendix 1). Other data are included under the details per task section below.

- **Determine the dose of BuOE2 that is most effective in reduction ROS, inhibiting NF-kB signaling, and inflammation in the spinal cord acutely post-SCI**
  We have completed approximately 100% of the animal experiments in support of this goal and anticipate full completion of the data analysis by March 2016. Thus far, the main finding is that the 0.1mg/kg dose is seemingly the most effective in reducing ROS and inflammation after SCI in the rodent models. Please see the data included under the details per task section, below.

- **Determine the dose of BUOe2 that is most effective in reducing SCI-induced neuropathic pain-like behaviors in mice**
  We have completed 100% of the animal experiment in support of this goal and are currently finishing the extensive data analysis required. We anticipate completion of the data analysis by March 2016.

- **Determine the dose of BuOE2 that is most effective in reducing SCI-induced neuropathic pain-like behaviors in rats**
  We have completed 100% of the animal experiment in support of this goal and are currently finishing the extensive data analysis required. We anticipate completion of the data analysis by March 2016.

- **Determine the effect of BuOE2 administration on cytokine/chemokine synthesis in the rat or mouse spinal cord**
  We have completed 100% of the animal experiment in support of this goal and are currently finishing the extensive data analysis required. We anticipate completion of the data analysis by March 2016.

- **Disseminate data concerning above to the medical and scientific community by publication in peer-reviewed journal and presentation at national meetings.**

  --As described above, the group submitted 1 manuscript (appendix 1). This manuscript is in revision for re-submission. We anticipate another 2 manuscript on these data will be submitted by June 2016.

  --A poster was presented at the 2015 International Symposium on Neural Regeneration by Dr. Lonnie Schneider (see appendix 1). We anticipate another 2 manuscripts submitted on this work by March 2016.

Accomplishments by the Specific Objectives of the SOW for Year 1 and Year 2 (note from approved revised SOW):

Year 1:

Task 1: Obtain required regulatory approval for project, including IACUC, Occupational Health Approval, and ACURO from UAB (Floyd and Tse) and from Duke (Warner, Batinic-Haberle, Spasojevic, Sheng). Months 1-3.

> This goal was achieved by IACUC ACURO approval completed by February 2014. Updated in March 2015 with new dosing scheme (see task 5, below for more details)

Task 2: Quantitatively assure purity of sufficient BuOE2 for use at both UAB and Duke for Year 1 *in vivo* studies. Order all necessary surgical supplies and biochemistry/ molecular reagents (ALL). Months 1-12.

> This goal was achieved. Purity of the compound was ensured by February 2014 and the research teams obtained necessary supplies to conduct the experiments detailed below.

Task 3: Order and acclimate adult male rats for evaluation in acute post-SCI time points related to Aim 1 at UAB (Floyd). Order and acclimate adult male mice and rats for BuOE2 subcutaneous pharmacokinetic studies (Warner and Spasojevic). Order and acclimate adult male mice for evaluation in acute post-spinal cord ischemia time points related to Aim 2 at Duke (Warner and Sheng). Months 3-12.

> This goal was achieved and the data obtained from these animals are detailed below with other tasks.

Task 4: Perform pharmacokinetic analysis at Duke (Batinic-Haberle and Spasojevic) in rats and mice treated with 0.1 mg/kg BuOE2 SQ. Rodents will be anesthetized and spinal cord, liver, and blood samples will be collected for measurement of BuOE2 at various time points post-injection (4 animals/species / time point). Months 3-12.

> This goal was achieved for the mice (See appendix 1) and is on-going for the rat, with nearly 50% completion. For this experiment, the uninjured rats or mice were given BuOE2 subcutaneously (SC) such that the animal received either one injection (single dose), or a single dose followed 3 days later by ½ the original dose (bi-weekly dose), or a single dose follow 7 days later by ½ the original dose (weekly). At the specified time point, animals were euthanized and the spinal cord, liver, and blood were collected for subsequent assessment of BuOE2 concentration. BuOE2 was extracted from organs and plasma in acetic acid and methanol using a Fast Prep apparatus followed by centrifugation. The levels of BuOE2 in plasma and organs were determined via high-performance liquid chromatography (HPLC) with a tandem mass spectrometer (MS/MS). As seen in figures 1 and 2, we determined that the bi-weekly dosing paradigm induced a significant and sustained tissue level of BuOE2 in the spinal cord.
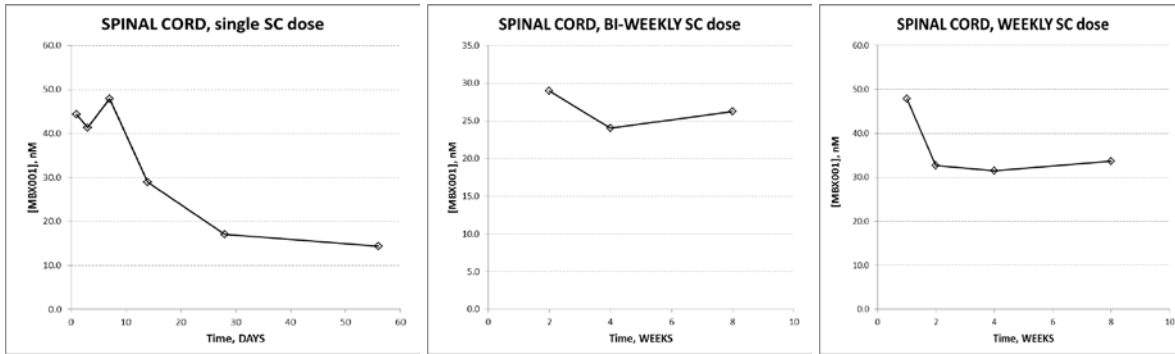
Figure 1: Effect of subcutaneous dosing on levels of BuOE2 (a.k.a. MBX001) murine spinal cord. Left panel shows the spinal cord level after a single dose of BuOE2 across several days post-injection. Middle panel shows the effect of a bi-weekly dose of BuOE2 on spinal cord levels measures across several weeks post-injection. Right panel shows the effect of a weekly dose of BuOE2 across several weeks.
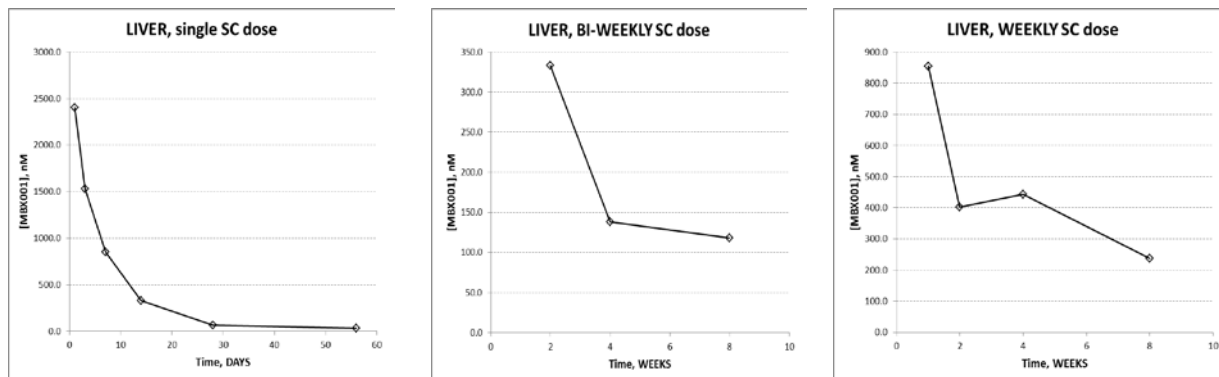

Figure 2: Effect of subcutaneous dosing on levels of BuOE2 (a.k.a. MBX001) murine liver. Left panel shows the spinal cord level after a single dose of BuOE2 across several days post-injection. Middle panel shows the effect of a bi-weekly dose of BuOE2 on spinal cord levels measures across several weeks post-injection. Right panel shows the effect of a weekly dose of BuOE2 across several weeks.

Task 5: For evaluation of ROS, NF-κB, and immunological markers at 24, 72 hr or 7 d post-SCI, induce C5 hemicontusion SCI in 225 male rats at UAB (Floyd) or spinal cord ischemia in 225 male mice at Duke (Warner and Sheng).   Months 3-12.

     a. Sham (all procedures except SCI): n=15
     b. SCI + vehicle: n=15
     c. SCI + 0.03mg/kg/day BuOE2: n=15
     d. SCI + 0.1mg/kg/day BuOE2: n=15
     e. SCI + 0.3mg/kg/day BuOE2: n=15

UPDATED TO:
     a. Sham (all procedures except SCI): n=15
     b. SCI + vehicle: n=15
     c. SCI + 0.2mg/kg loading dose; 0.1mg/kg/day BuOE2 daily: n=15
     d. SCI + 1.0 mg/kg loading dose; 0.5mg/kg/day BuOE2 weekly: n=15

e. SCI + 1.0 mg/kg loading dose; 0.5mg/kg/day BuOE2 daily: n=15

Due to the concerns with the lack of robust effects seen with the early dosing paradigm, we submitted a request to change the dosing scheme in March 2015. This request was approved and we therefore subsequently evaluated these higher doses. This change in the research plan cause modest delays in the progress, but we anticipate the completion of these associated tasks in 2016.

This task is completed in that 100% of the animal work is completed and data analysis on-going subsequent to the induction of SCI is on-going. As planned, experimental hemicontusion SCI surgery in the rat was performed at UAB and experimental ischemic SCI in the mice was being performed at Duke. There has been no change from the injury model as described in the original application. Briefly for induction of SCI in the rat, male Sprague-Dawley rats (250-275g) were anesthetized with inhaled isoflurane and body temperature was maintained at 37C. The mid-cervical vertebral column was exposed and a bilateral laminectomy was performed at vertebral level C5. A moderate (300kdyne) contusion injury was be administered using the Infinite Horizons impactor. For induction of SCI in the mouse, male C57BL/6J mice were anesthetized with isoflurane and placed in the right lateral decubitus position. A left thoracotomy was performed by cauterizing the superficial layer of the intercostal muscle, then inserting the tip of a closed surgical scissor into the thoracic cavity and gently widening the intercostal space by opening the scissor. The thoracic aorta was visualized and a small aneurysm clip was placed on the aorta at the level of T8 to induce ischemic injury. The clip was removed after 10 min.

Task 6: At 24, 48 hours, or 7 days post-SCI, exsanguinate a subset of the rats at UAB (Floyd and Tse) or mice at Duke (Warner and Sheng) and rapidly remove and freeze the spinal cord tissue. Next, prepare tissue samples and lysates for subsequent biochemical and molecular analysis and send to Tse lab at UAB (Floyd, Warner, Sheng). Months 3-12.

This task has been 100% completed in that all spinal cords have been extracted, frozen and prepared for subsequent analysis.

Task 7: At 24, 48 hours, or 7 days post-SCI, exsanguinate a subset of the rats at UAB (Floyd and Tse) or mice at Duke (Warner and Sheng) and rapidly fix tissue with 4% paraformaldehyde. Remove the spinal cord, cryoprotect, and then block/ freeze the spinal cord segments for subsequent cryosectioning. Collect serial cryosections of the spinal cord for subsequent histochemical and immunohistochemical analysis at UAB and Duke (Floyd, Warner, Sheng). Months 3-12.

This task has been 100% completed in that all spinal cord have been extracted, fixed, and subsequently cryo-sectioned.

Task 8: At 24, 48 hours, or 7 days post-SCI, exsanguinate a subset of the rats (Floyd and Tse) or mice (Warner and Sheng) and freeze for subsequent purification of microglia cells and astrocytes from spinal cord tissue by discontinuous percoll gradients or with magnetic beads conjugated to microglia (CD11b)- or astrocyte (GLAST/ACSA-1)-specific antibodies. Conduct flow cytometry experiments from extracted rat or mouse microglia and astrocytes to detect ROS using redox-sensitive dyes and pro-inflammatory cytokines with fluorochrome-conjugated antibodies (Tse). Months 3-12.

All of the tissue extraction and purification steps have been completed. We are in the process of optimizing the flow cytometry experiments thus that portion of the task is on-going making this task 50% complete.

Task 9: Evaluate pro-inflammatory cytokine/chemokine synthesis in rat or mouse spinal cord protein lysates with a Luminex Beadlyte 21-plex multi-cytokine detection system (Tse). Months 3-12.

This task has been completed for the rat at the 24 hour time point, as detailed below. With regard to the mouse experimentation, all samples have been collected and prepared as lysates for the multi-cytokine detection system. We are currently optimizing the detection for the mouse tissue and then can complete the assay. Analysis for both species is on-going. This task is on-going, with an estimated completion of 80%. Thus far, we have preliminarily assessed the effect of BuOE2 administration on pro-inflammatory signals tumor necrosis factor alpha (TNFα) and interleukin 6 (IL-6) in the rodent spinal cord at 24 hours post-SCI using enzyme-linked immunosorbent assays (ELISA) for cytokine detection (R&D Systems, TNF alpha DuoSet #DY510; R&D systems IL-6 DuoSet #DY506) . Experimental SCI and post-SCI administration of BuOE2 was induced in the rats and mice as described above. Spinal cord segments from the epicenter and one segment rostral (above the injury level, toward the head) and caudal (below the injury level, toward the tail) of the epicenter were also collected and assessed. Extracted spinal cord was snap frozen and then subsequently homogenized. All values are normalized to protein level and readings are within the standard curves.
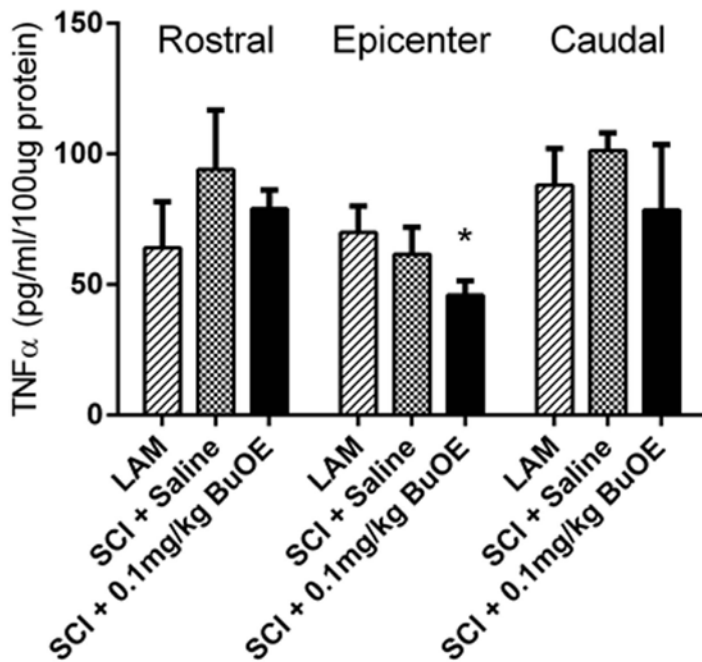
Figure 3: Effect of BuOE2 on expression of TNFα in the rat spinal cord at 24 hours post-SCI. In the rostral and caudal segments, SCI induced an elevation in TNFα as compared to the uninjured control (LAM) that was reduced in the groups administered BuOE2. The reduction in TNFα levels in the BuOE2 group as compared to the SCI + saline group reached statistical significance for tissue at the epicenter of the lesion (*).

Preliminary evaluation of the effect of SCI and post-SCI administration of BuOE2 on TNFα levels at 24 hours post-SCI in the rat is shown in figure 3. We found that SCI induced an increase in the levels of TNFα, particularly in the rostral and caudal segments and that post-SCI administration of BuOE2 reduced levels of TNFα as compared to the SCI+ saline group in tissue at the epicenter. We next evaluated the effect of SCI and post-SCI administration of BuOE2 on IL-6 levels at 24 hours post-SCI in the rat, figure 4. As with TNFα, we found that SCI caused an increase in the levels of Il-6 in the spinal cord (comparisons between LAM and SCI + saline groups). We also observed that levels of Il-6 were reduced in tissue from the group of animals that received BuOE2 post-SCI. With regard to the murine ischemic SCI, we did not find robust differences between groups for the levels of TNFα at 24 hours post-SCI (figure 5). However, when the levels of Il-6 were evaluated in the murine ischemic injury model (figure 6), we found that injury caused an increase Il-6 (comparisons between Sham (lam) and SCI + saline groups). Also, we observed that post-SCI administration of BuOE2 reduced the levels of IL-6, both at the 0.1mg/kg and the 0.3mg/kg group. Additional doses and time points are currently being evaluated to complete this data set and confer a more complete understanding of these effects.
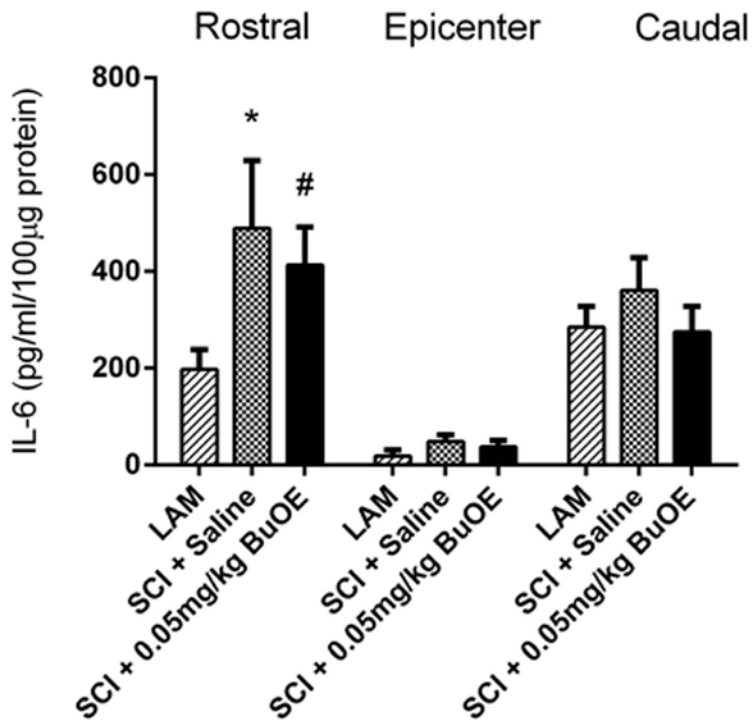
Figure 4: Effect of BuOE2 on expression of Il-6 in the rat spinal cord at 24 hours post-SCI. In the rostral and caudal segments, SCI induced an elevation in Il-6 as compared to the uninjured control (LAM) that reached statistical significant in the rostral segments (*). The levels of Il-6 were reduced in the groups administered BuOE2 as compared to the SCI + saline groups. This reduction reached statistical significance for tissue rostral to the epicenter of the lesion (#).
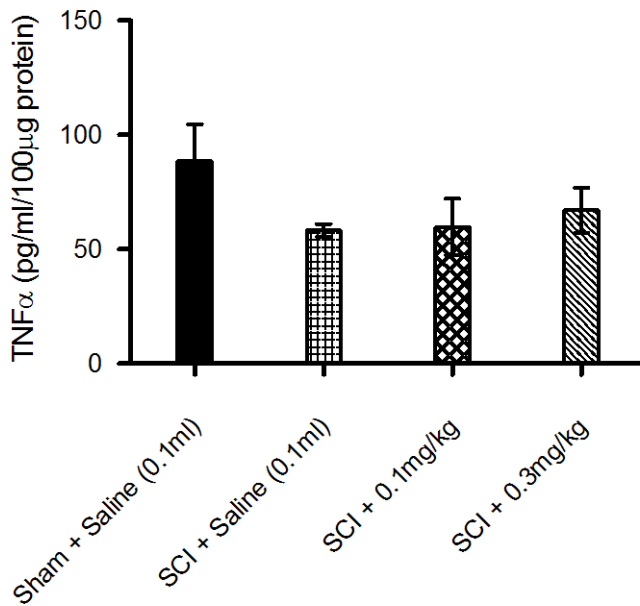

Figure 5: Effect of BuOE2 on expression of TNFα in the murine spinal cord at 24 hours post-SCI. No robust changes in TNFα levels were seen across treatment groups.
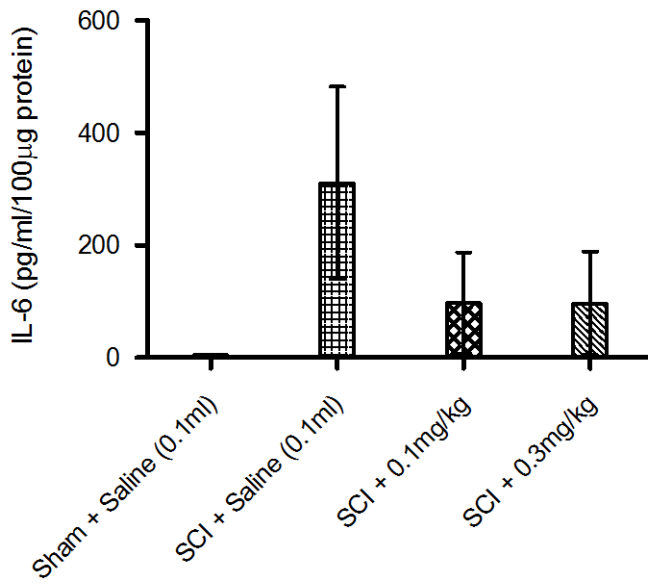
Mouse SCI - 24h after thoracic aorta clamping

Figure 6: Effect of BuOE2 on expression of Il-6 in the murine spinal cord at 24 hours post-SCI. SCI induced an elevation in Il-6 as compared to the uninjured control (sham). The levels of Il-6 were reduced in the groups administered BuOE2 as compared to the SCI + saline groups.

We next used the multiplex chemokine system to assess the effect of SCI and BuOE2 treatment on several inflammation biomarkers in tissue extracted from the lesion epicenter and in segments rostral and caudal to the lesion epicenter. Note that these experiment groups received the higher doses from the revised dosing scheme. Data from the multiplex in tissue extracted at 24hours post-SCI is shown in figures 7- 28 with each figure legend describing the relevance of the biomarker assessed. We found the following changes to be of
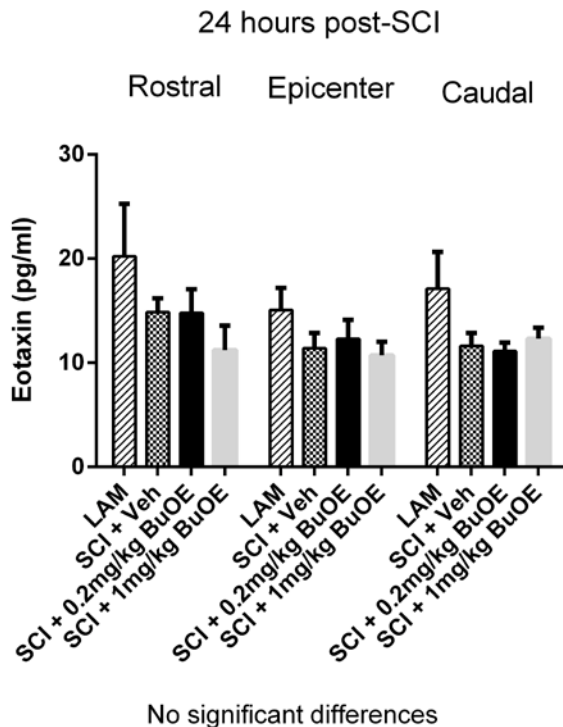
24 hours post-SCI

Figure 7: Effect of BuOE2 on expression of eotaxin in the rat spinal cord at 24 hours post-SCI. Eotaxins are in the chemokine subfamily of eosinophil chemotactic proteins that includes CCL11. No significant differences between groups were found.
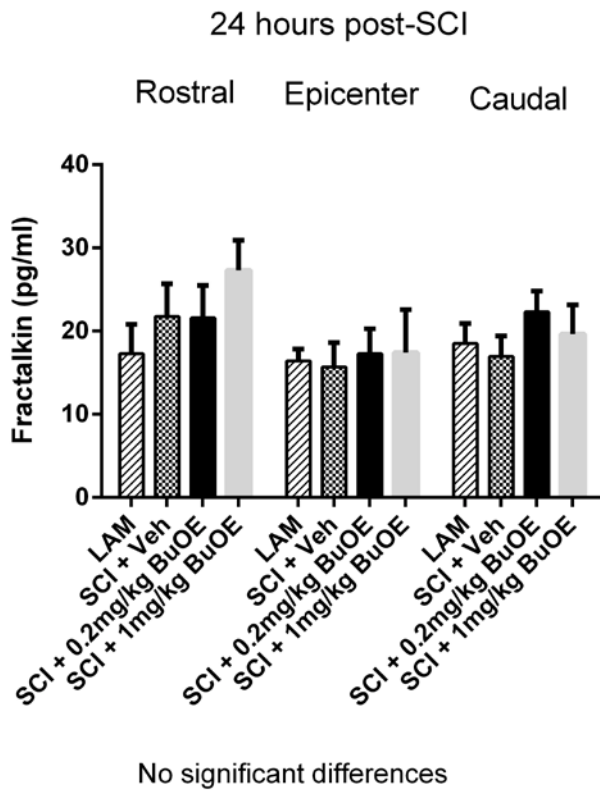
24 hours post-SCI

Figure 8: Effect of BuOE2 on expression of fractalkin in the rat spinal cord at 24 hours post-SCI. Fractalkine (CX3C) is a chemokine which is thought to chemo-attract T cells and monocytes. No significant differences between groups were found.

No significant differences

24 hours post-SCI

Figure 9: Effect of BuOE2 on expression of G-CSF in the rat spinal cord at 24 hours post-SCI. Granulocyte colony stimulating factor (G-CSF) is a glycoprotein that stimulates an immune response. No significant differences between groups were found.

No Significant Differences

24 hours post-SCI

Rostral Epicenter Caudal

No significant differences
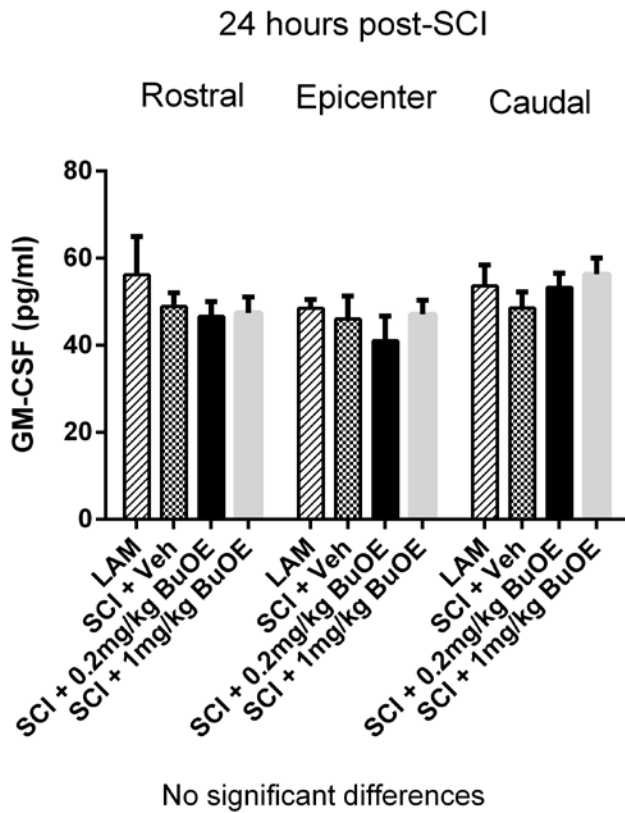
Figure 10: Effect of BuOE2 on expression of GM-CSF in the rat spinal cord at 24 hours post-SCI. Granulocyte macrophage colony stimulating factor (GM-CSF) is a glycoprotein that stimulates an immune response. No significant differences between groups were found.

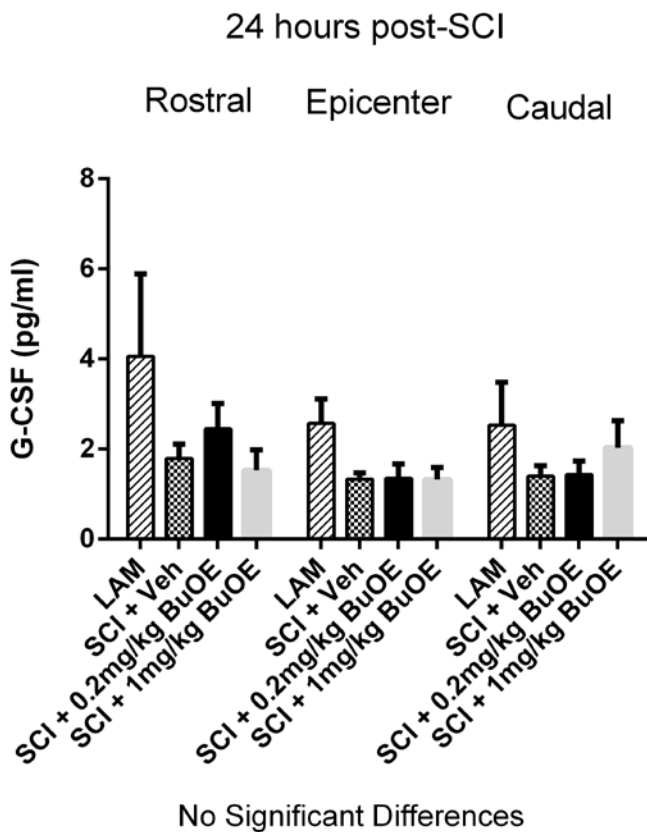## 24 hours post-SCI

Rostral Epicenter Caudal

No significant differences

Figure 11: Effect of BuOE2 on expression of IL-1α in the rat spinal cord at 24 hours post-SCI. IL-1α is a protein of the interleukin 1 family that regulates the immune response. No significant differences between treatment groups were found, although a significant induction following SCI was observed.

24 hours post-SCI

Rostral   Epicenter   Caudal

No significant differences

Figure 12: Effect of BuOE2 on expression of IL-2 in the rat spinal cord at 24 hours post-SCI. IL-2 is a protein of the interleukin family that regulates the immune response. No significant differences between treatment groups were found, although a significant reduction following SCI was observed with a trend toward an drug effect for the 0.2 and 1.0 mg/kg dose at the rostral and epicenter segments.
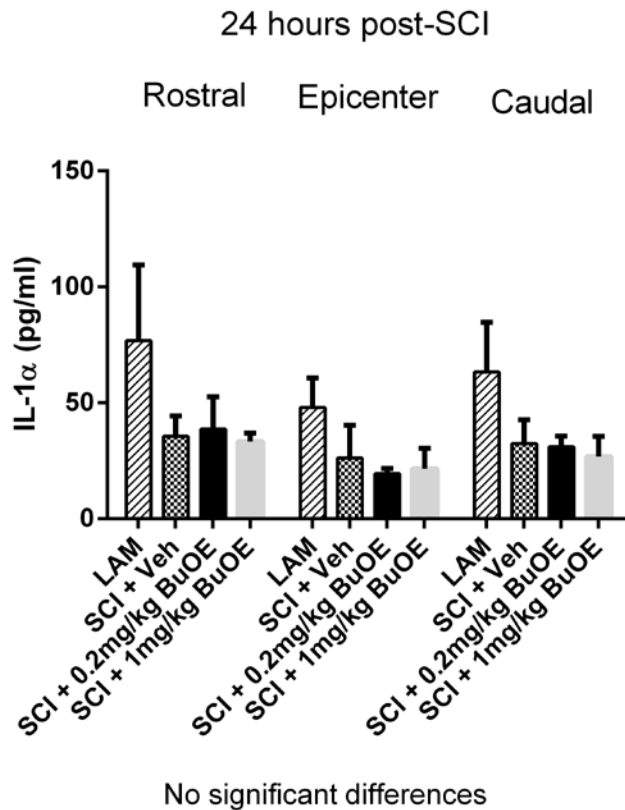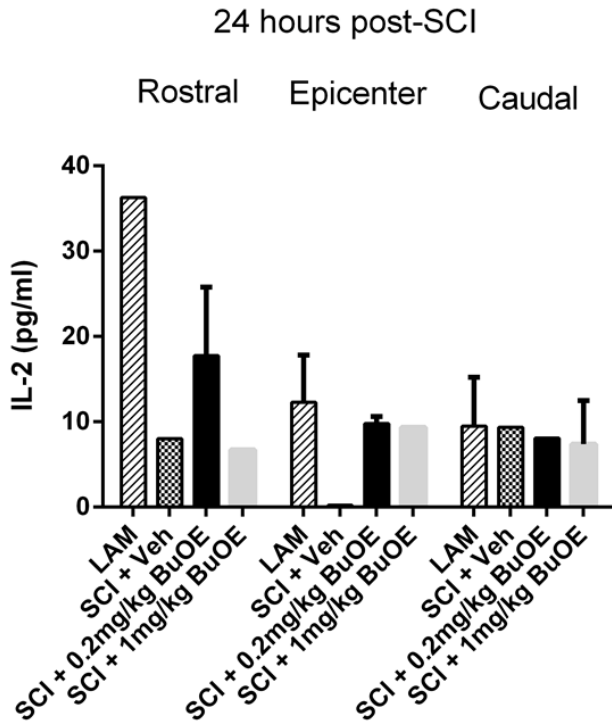
24 hours post-SCI

Rostral   Epicenter   Caudal

No significant differences

Figure 13: Effect of BuOE2 on expression of IL-4 in the rat spinal cord at 24 hours post-SCI. IL-4 is a protein of the interleukin family that regulates the immune response. No significant differences between treatment groups were found, although a significant reduction following SCI was observed with a trend toward a drug effect for the 0.2 and 1.0 mg/kg dose at the rostral and caudal segments.

24 hours post-SCI

Rostral   Epicenter   Caudal

No significant differences
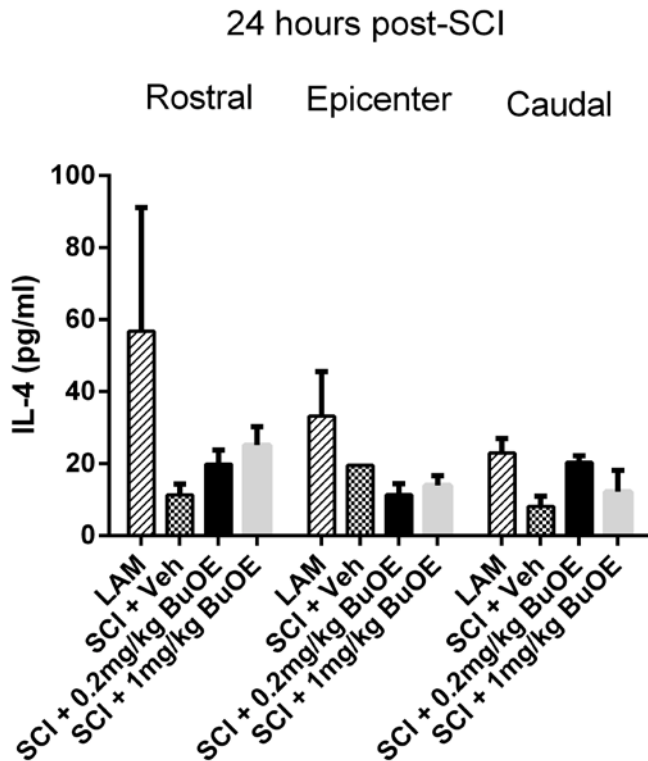
Figure 14: Effect of BuOE2 on expression of IL-5 in the rat spinal cord at 24 hours post-SCI. IL-5 is a protein of the interleukin family that regulates the immune response. No significant differences between treatment groups were found.

24 hours post-SCI

Rostral   Epicenter   Caudal

no significant differences

Figure 15: Effect of BuOE2 on expression of IL-10 in the rat spinal cord at 24 hours post-SCI. IL-10 is a protein of the interleukin family that regulates the immune response. In the rostral and caudal segments, a significant reduction in IL-10 was observed following SCI. Also, there was an trend toward effect of 0.2mg/kg BuOE2 in the rostral segment.

24 hours post-SCI

Rostral   Epicenter   Caudal

No significant differences

Figure 16: Effect of BuOE2 on expression of IL-17a in the rat spinal cord at 24 hours post-SCI. IL-17a is a protein of the interleukin family that regulates the immune response. No significant differences between treatment groups were found.

24 hours post-SCI

Rostral   Epicenter   Caudal

*p<0.01 SCI 1mg/kg BuOE Epicenter vs. Caudal
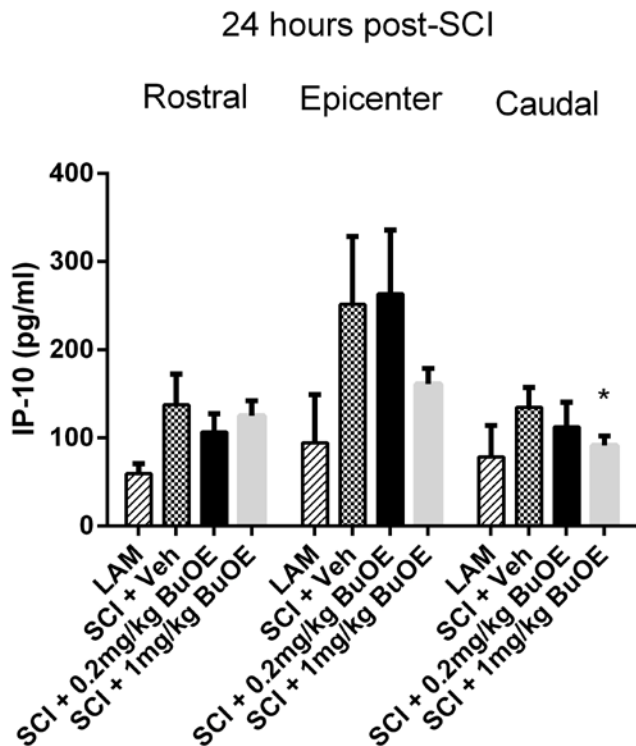
Figure 17: Effect of BuOE2 on expression of IP-10 in the rat spinal cord at 24 hours post-SCI. Interferon gamma-induced protein 10 is an inducible cytokine that activates the immune response. Trends were observed in relation to an upregulation following SCI with some effect of BuOE observed.

24 hours post-SCI

Rostral   Epicenter   Caudal
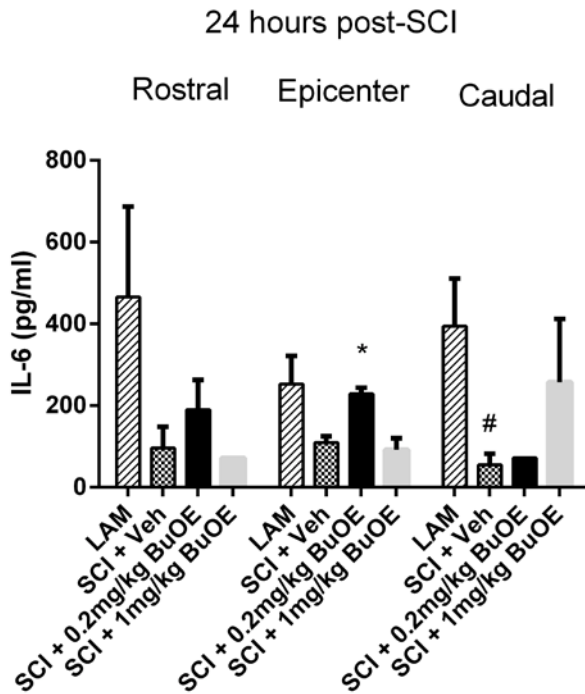
* p<0.01 SCI vs. SCI 0.2mg/kg BuOE
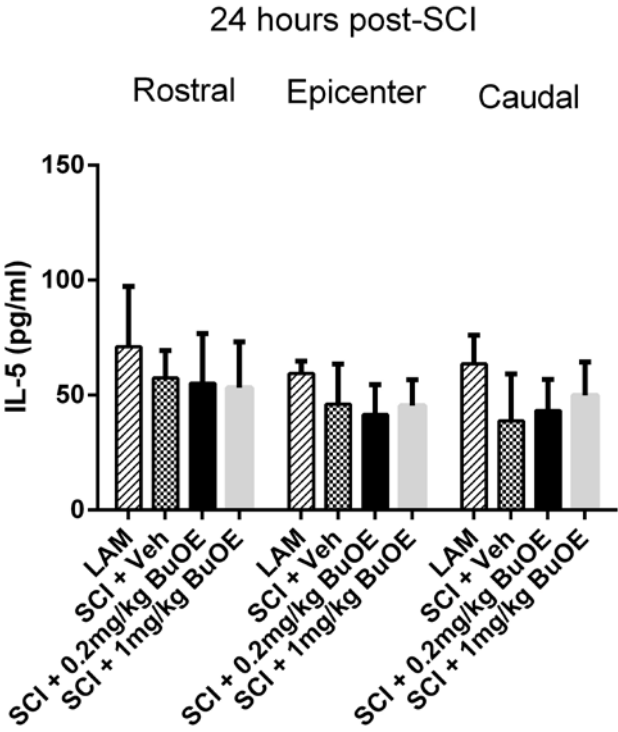
p=0.05 LAM vs.SCI

Figure 18: Effect of BuOE2 on expression of IL-6 in the rat spinal cord at 24 hours post-SCI. IL-6a is a protein of the interleukin family that regulates the immune response. A reduction following injury was observed as were some effects of BuOE treatment.

24 hours post-SCI

Rostral   Epicenter   Caudal
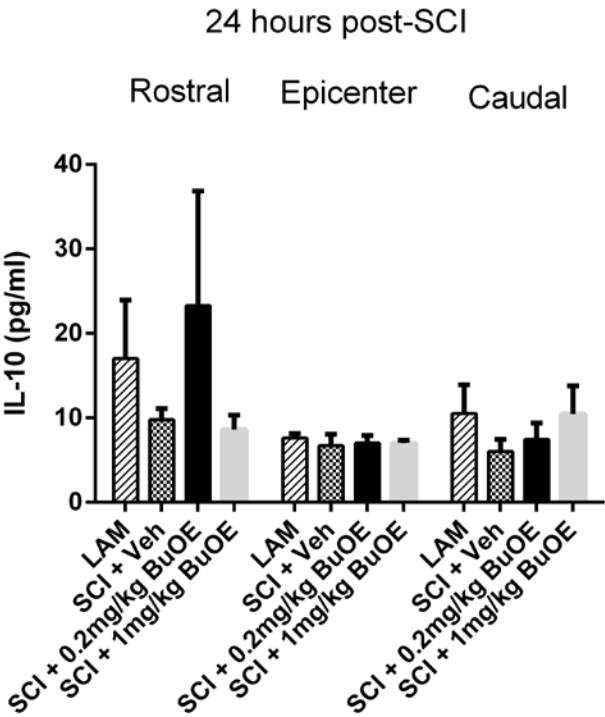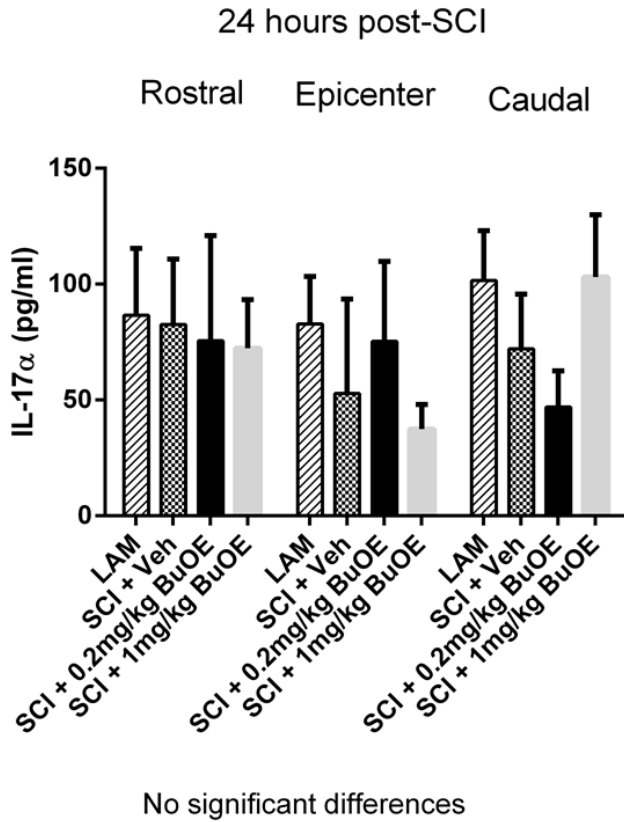

*p<0.05 LAM vs. SCI

Figure 19: Effect of BuOE2 on expression of IL-18 in the rat spinal cord at 24 hours post-SCI. IL-18 is a protein of the interleukin family that regulates the immune response. A upregulation following injury was observed as were some effects of BuOE treatment.

24 hours post-SCI

Rostral   Epicenter   Caudal

*p<0.05 LAM vs. SCI + Veh

Figure 20: Effect of BuOE2 on expression of MCP-1 in the rat spinal cord at 24 hours post-SCI. Monocyte chemotactic protein 1(MCP1) is an inducible cytokine that is pro-inflammatory. An upregulation following injury was observed as were some effects of BuOE treatment

24 hours post-SCI

Rostral   Epicenter   Caudal

* p<0.01 SCI vs. SCI 1mg/kg BuOE

Figure 21: Effect of BuOE2 on expression of EGF in the rat spinal cord at 24 hours post-SCI. Epidermal growth factor (EGF) is a protein that supports cell proliferation. An upregulation following injury was observed in the epicenter and caudal segment, as were some effects of BuOE treatment

24 hours post-SCI

Rostral   Epicenter   Caudal
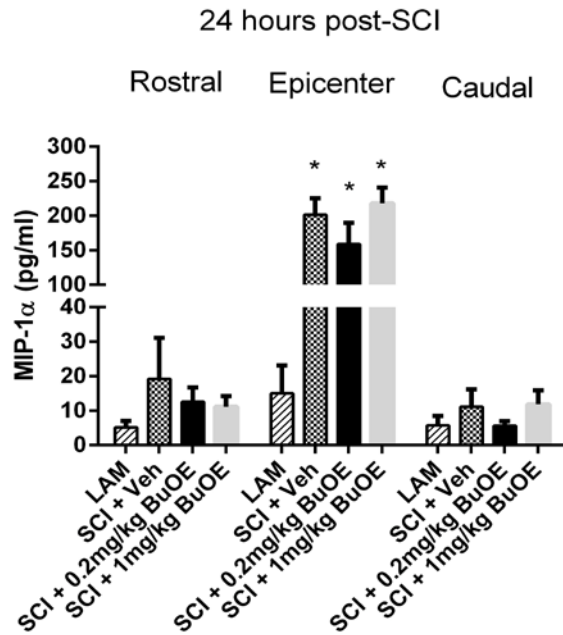
* p<0.01 LAM vs SCI

Epicenter SCI groups are all significant compared to rostral and caudal

No drug effect

Figure 22: Effect of BuOE2 on expression of MIP-1a in the rat spinal cord at 24 hours post-SCI. Macrophage inflammatory protein 1A is a protein that recruits inflammatory cells. An upregulation following injury was observed in the epicenter and caudal segment.

24 hours post-SCI

Rostral   Epicenter   Caudal
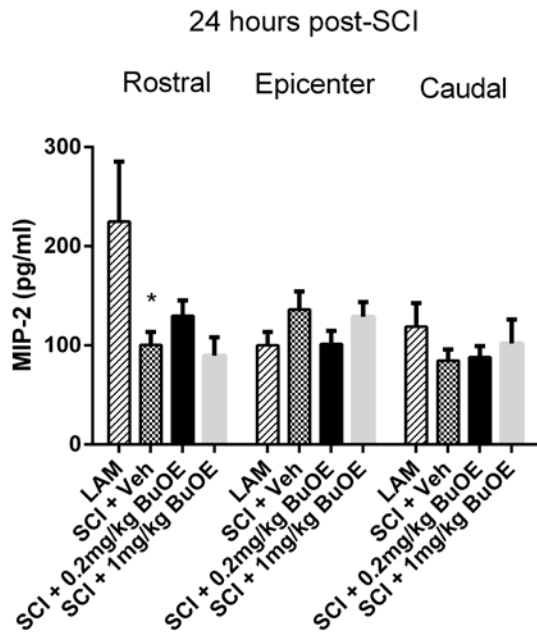
*p<0.05 LAM vs SCI

Figure 22: Effect of BuOE2 on expression of MIP-1a in the rat spinal cord at 24 hours post-SCI. Macrophage inflammatory protein 2 is a protein that recruits inflammatory cells. An downregulation following injury was observed in the rostral segment.
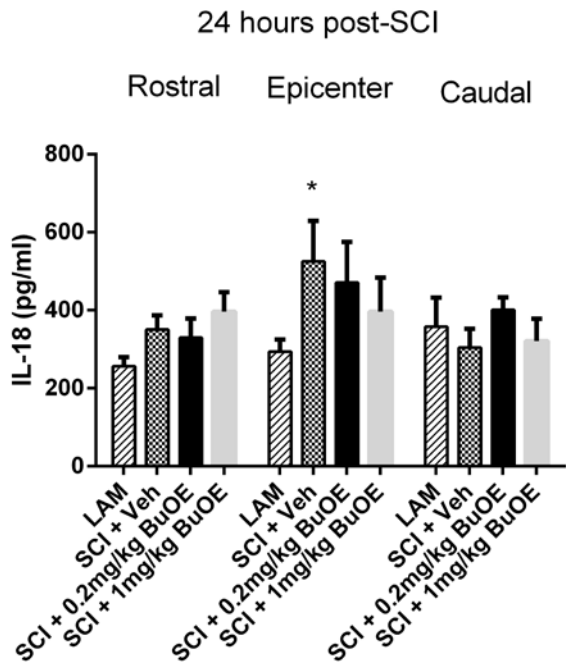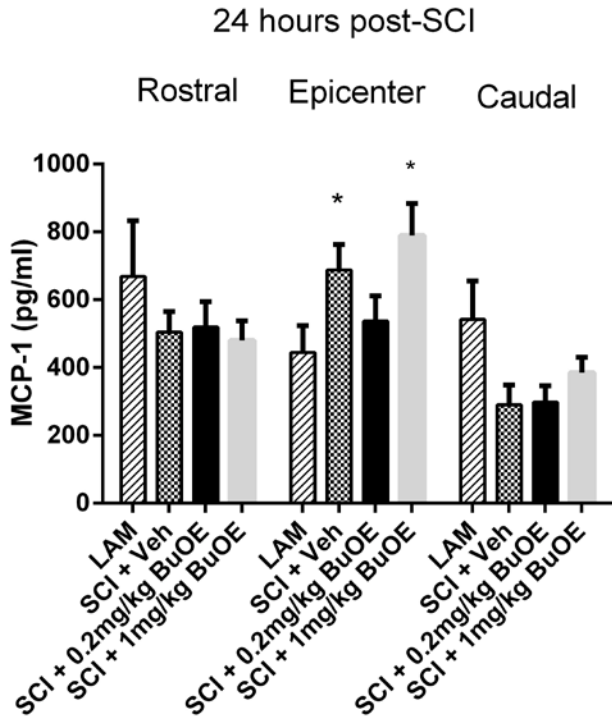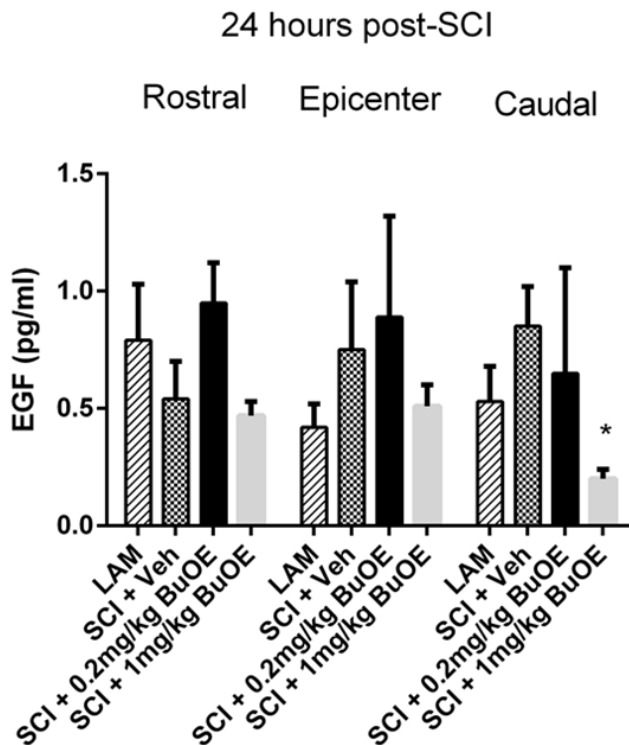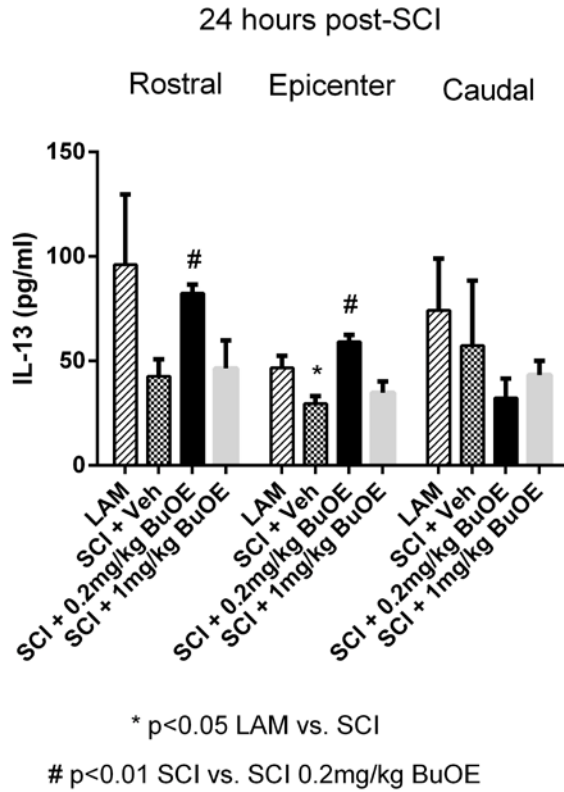
Figure 23: Effect of BuOE2 on expression of IL-13 in the rat spinal cord at 24 hours post-SCI. IL-13 is a protein of the interleukin family that regulates the immune response. A reduction following SCI was observed as well as effects of BuOE in the rostral and caudal segments.
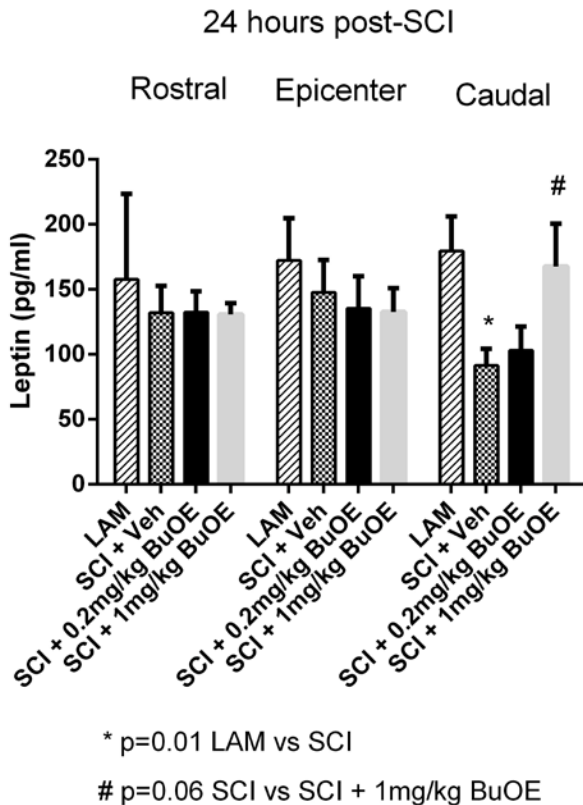
Figure 24: Effect of BuOE2 on expression of leptin in the rat spinal cord at 24 hours post-SCI. Leptin is a hormone which regulates energy homeostasis. A reduction following SCI was observed as well as effects of BuOE in the caudal segment.

24 hours post-SCI

Rostral   Epicenter   Caudal

*p<0.01 SCI vs SCI 0.2mg/kg BuOE

#p<0.01 0.2mg/kg BuOE Epicenter vs. Caudal
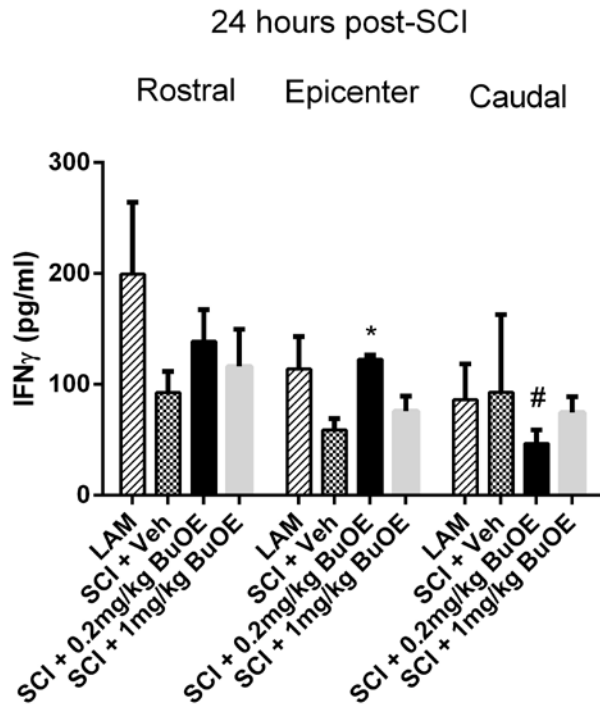
Figure 25: Effect of BuOE2 on expression of IFNy in the rat spinal cord at 24 hours post-SCI. Interferon gamma (IFNy) is a cytokine which regulates immune function. A reduction following SCI was observed as well as effect of BuOE in the caudal segment.

24 hours post-SCI

Rostral   Epicenter   Caudal

* p=0.02 LAM vs. SCI
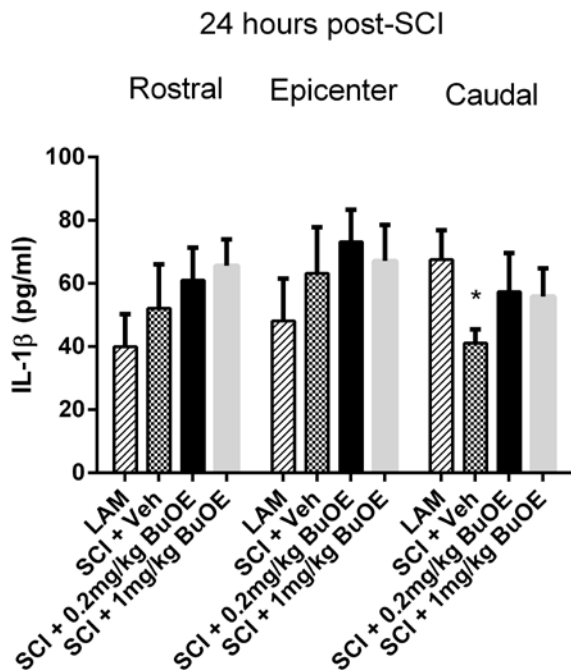
Figure 26: Effect of BuOE2 on expression of IL-1B in the rat spinal cord at 24 hours post-SCI. IL-1B is a protein of the interleukin family that regulates the immune response. A reduction following SCI was observed in the caudal segment, but no drug effects.
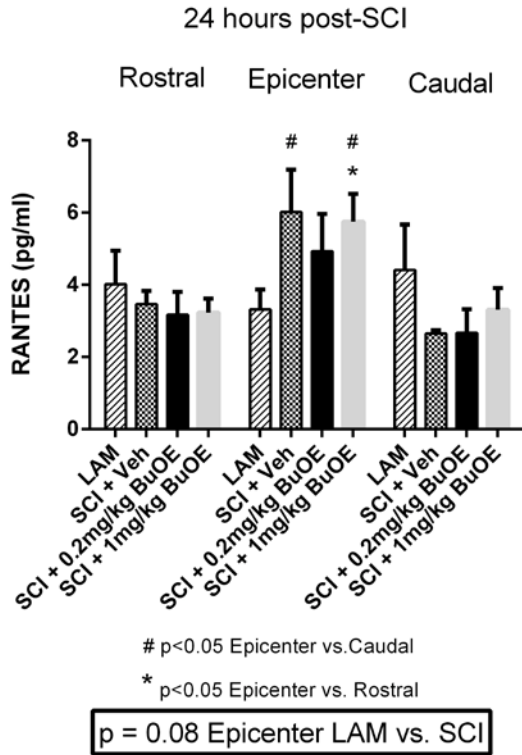
Figure 27: Effect of BuOE2 on expression of RANTES in the rat spinal cord at 24 hours post-SCI. Regulated on activation normal T cell expressed and secreted (RANTES) protein recruits immune cells to the injury site. An upregulation following SCI was observed in the epicenter, but no drug effects.
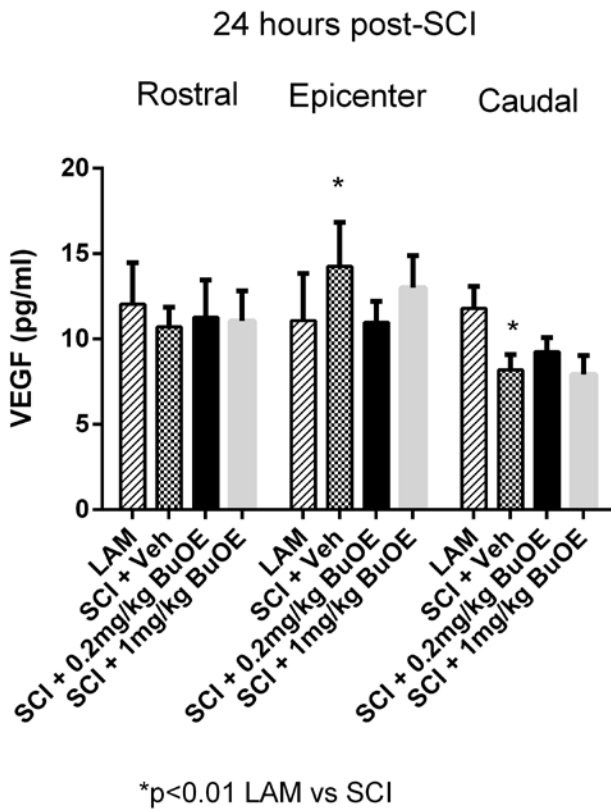
Figure 28: Effect of BuOE2 on expression of VEGF in the rat spinal cord at 24 hours post-SCI. Vascular endothelial growth factor (VEGF) stimulates a response to restore oxygen to a damaged system. An upregulation following SCI was observed in the epicenter and a downregulation in the caudal segment, but no drug effects.

particular interest: a) several protein in the interleukin family including IL-4, IL-6, IL-10, IL-13 as well as IFN-γ; b) proteins which are chemoattractant including RANTES, MCP-1, MIP-1α; and c) proteins that regulate cellular energetics including Leptin and VEGF. We plan to continue these experiments by examining other acute time points as proposed.

Task 10: Conduct immunoblotting on extracts from rat and mouse spinal cord sections to evaluate activation of NF-κB and post-translational modification of NF-κB subunits (Tse). Months 3-12.

This task is on-going. Standardized protocols between the collaborative research team have been established and tissue samples have been effectively prepared according to these protocols. The tissue extraction completion parallels the task 5 completion, and is currently 100% complete.

We are continuing the evaluation of NF-kB signaling post-SCI in the rat. For this experiment, rats were injured and administered BuOE2 after SCI as described above. Spinal cords were extracted at 24h post-SCI, flash frozen, and then homogenized. Tissue was also fractionated using the Active Motif Nuclear Extraction King (catalog #40010) to obtain nuclear fractions. Next, immunoblots were conducted to assess level of total NF-kB (p65, Cell Signaling antibody #8242s) and activated NF-kB (phosphorylated p65, Cell Signaling antibody #3033S). GAPDH (Protein Tech antibody # HRP-6004) was used as a loading control and all protein values as
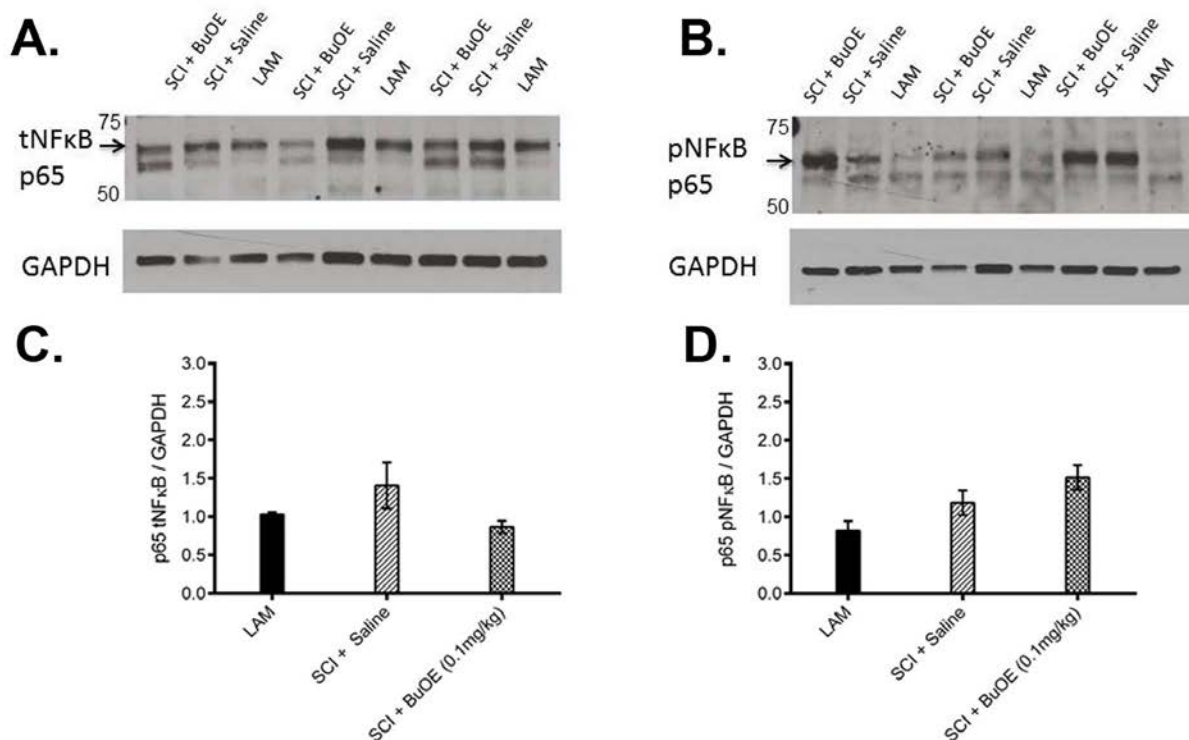
Figure 29: Effect of post-SCI administration of BuOE2 on NF-kB signaling at 24 hours post-injury in the rats. All analyses were conducted at the epicenter of the spinal cord lesion. Panel A is a representative immunoblot probing for total NF-kB (p65) from spinal cord tissue homogenates taken from 9 animals with the group of the animal listed above each lane. GPADH was used as a loading control and the immunoblot corresponding to the lane above is pictured. Panel B is a representative immunoblot probing for phosphorylated (activated) NF-kB (p65) from spinal cord tissue homogenates taken from 9 animals with the group of the animal listed above each lane. GPADH was used as a loading control and the immunoblot corresponding to the lane above is pictured. Panel C is quantification using relative optical density of the total NF-kB protein in the nuclear fraction (from A) protein normalized to GAPDH. Panel D is quantification using relative optical density of the phosphorylated NF-kB protein in the nuclear fraction normalized to GAPDH.

assessed by relative optical density were normalized to GAPDH. Also, each immunoblot included tissue extracts from control (laminectomy only), SCI + vehicle (saline) and SCI + BuOE2 such that comparisons between experimental groups could be done between samples on the same immunoblot. As seen in figure 29, preliminary data indicate that post-SCI administration of BuOE2 induces a reduction in the level of total NF-kB in the nuclear fraction. With regard to activated NF-kB as detected by phosphorylation at the p65, no difference between injury groups were observed, suggesting that post-SCI BuOE2 may not affect activation of this subunit. Subsequent experiments will follow up on these preliminary findings in both rats and mice.

YEAR 2:
Task 1: Obtain required regulatory approval for project, including IACUC, Occupational Health Approval, ACURO from UAB (Floyd and Tse) and from Duke (Warner, Batinic-Haberle, Spasojevic, Sheng). Month 1.

This goal was achieved by IACUC ACURO approval annual renewal was completed by March 2015 with new dosing scheme (see task 5, below for more details)

Task 2: Quantitatively assure purity of sufficient BuOE2 for use at both UAB and Duke for Year 2 *in vivo* studies. Order all necessary surgical supplies and biochemistry/ molecular reagents (ALL). Months 1-12.

This task was completed.

Task 3: Order and acclimate adult male rats for evaluation in chronic post-SCI time points related to Aim 1 at UAB (Floyd). Order and acclimate adult male mice for evaluation in chronic post-SCI time points related to Aim 2 at Duke (Warner and Sheng). Months 2-12.

This task was completed.

Task 4: For evaluation of neuropathic pain and functional recovery as well as the assessment of ROS, NF-κB, and immunological markers at 6 weeks post-SCI, induce C5 hemicontusion SCI in 100 male rats at UAB (Floyd) or conduct 10 min aortic occlusion in 100 male mice at Duke (Warner and Sheng). Months 2-12.

This task was completed and all rodent animal experimentation related to the chronic time point has been conducted.

Task 5: Evaluate the effect of BuOE2 administration on neuropathic pain by assessing the daily incidence of dermatome-specific over-grooming, weekly assessment of tactile allodynia using Von Frey hairs, weekly assessment of thermal cold allodynia using the acetone test in rats at UAB (Floyd) and mice at Duke (Sheng). Months 2-12.
    a. Sham (all procedures except SCI): n=20
    b. SCI + vehicle: n=20
    c. SCI + 0.2mg/kg loading dose; 0.1mg/kg daily BuOE2: n=20
    d. SCI + 1.0mg/kg loading dose; 0.5mg/kg weekly BuOE2: n=20
    e. SCI + 1.0mg/kg loading dose; 0.5mg/kg daily BuOE2: n=20

The animal work for this task is 100% completed. All assessments are in the data analysis stage which included scoring the outcomes and statistical evaluations. Evaluations and data analysis should be completed by June 2016.

Task 6: Evaluate the effect of BuOE2 administration on functional recovery by weekly evaluation of forepaw use in skilled and unskilled use tests and locomotion tasks in rats at UAB (Floyd) and measurement of rotarod performance, and Basso mouse scale in mice at Duke (Sheng). Months 2-12.

The animal work has been completed and the data is currently being scored. Evaluations and data analysis should be completed by June 2016.

Task 7: At 6 weeks post-SCI, exsanguinate a subset of the rats at UAB (Floyd) or mice at Duke (Sheng) and rapidly remove and freeze the spinal cord tissue. Transfer samples to Tse lab at UAB (Floyd and Sheng). Next, prepare tissue samples and lysates for subsequent biochemical and molecular analysis (Tse). (n=6/group). Months 2-12.

This task is complete. The animal work is 100% complete and all the tissues have been collected and transferred to UAB. Lysates have been prepared.

Task 8: At 6 weeks post-SCI, exsanguinate a subset of the rats at UAB (Floyd) or mice at Duke (Sheng) and rapidly fix tissue with 4% paraformaldehyde. Remove the spinal cord, cryoprotect, and then block/ freeze the spinal cord segments for subsequent cryosectioning. Collect serial cryosections of the spinal cord for subsequent histochemical and immunohistochemical analysis at UAB and Duke(Floyd and Sheng). (n=6/group) Months 2-12.

This task is complete. The animal work is 100% complete and all the tissues have been collected, blocked and frozen.

Task 9: In a subset of the rats at UAB (Floyd) or mice at Duke(Sheng), extract the spinal cord for measurement of BuOE2 tissue concentration. Send samples to Spasojevic lab at Duke (Floyd and Sheng). Measure concentration of BuOE2 in spinal cord and blood from samples at Duke(Spasojevic). (n=6/group). Months 2-12.

The animal work for this task has been completed. The analysis of the samples remains, making this task 50% complete.

Task 10: Conduct flow cytometry experiments on spinal cord microglia and astrocyte cells from extracted rat or mouse tissue to detect ROS using redox-sensitive dyes and pro-inflammatory cytokines with fluorochrome-conjugated antibodies at UAB (Tse). Months 2-12.

We are containing to optimize these procedures for the spinal cord tissue; thus, this task is on-going.

Task 11: Evaluate pro-inflammatory cytokine/chemokine synthesis in rat or mouse spinal cord protein lysates with a Luminex Beadlyte 21-plex multi-cytokine detection system at UAB (Tse). Months 2-12.

The animal work related to this task is completed and the tissue samples have been collected. The detection experiments are on-going and at 30% completion. We anticipate completion of all experimentation and of data analysis by June 2016.

Task 12: Conduct immunoblotting on extracts from rat or mouse spinal cord sections to evaluate activation of NF-κB and post-translational modification of NF-κB subunits at UAB (Tse). Months 2-12.
The animal work related to this task is completed and the tissue samples have been collected. The detection experiments are on-going and at 30% completion. We anticipate completion of all experimentation and of data analysis by June 2016.

4. IMPACT

Development of the principal disciplines: The work thus far has had an impact in developing and extending our knowledge on the dose of BuOE2 that results in a steady level in the spinal cord in rodents. Secondly, these studies have begun to examine the effects of post-SCI administration of BuOE2 on inflammation and NF-κB signaling in the spinal cord tissue after contusion and ischemic injury in rodent models.

Other disciplines: The knowledge concerning the dosing and tissue accumulation of BuOE2 will have an impact on other disciplines in which a therapeutic compound of this type could be used, including but not limited to traumatic brain injury, stroke, alleviation of chemotherapy-induced pain, and diabetic neuropathy.

Technology transfer: Nothing to report.

Society: Nothing to report.

5. CHANGES/ PROBLEMS:

Changes in approach:

1) Initially we proposed to evaluate lower doses of BuOE. However, our preliminary data indicated that these doses were too low which caused us to submit a change in the statement of work to evaluate higher doses. Additionally, our initial preliminary data suggested that either a weekly or daily dosing schedule would lead to differentially accumulated concentration of drug in the spinal cord with weekly achieving a steady state and daily causing an escalating dosing. As we are not sure which spinal cord drug concentration is the best for protection, we updated the statement of work to compare both strategies.

2) There is concern in the rodent literature that exclusive use of reflexive paw withdrawal data to indicate pain is not preferred. Thus, we propose to add a subsequent analysis of facial grimace in rats. Our preliminary data indicate that grimace can be used to evaluate both spontaneous pain and evoked pain. We have recorded the facial expression of rats during the acetone test and propose to evaluate these data as an additional pain marker. There will be no increase in animal number or budget to conduct this additional pain assessment.

Problems and delays with plan to resolve:

1) Due to the approved change in the dosing scheme, we are modestly behind in achieving our objectives in the rodent research. However, all the animal experimentation related to rodents has been completed and we are confident that we can complete the necessary data analysis the two quarters or 2016.

Changes with impact on expenditures: Nothing to report.

Changes in use and care of vertebrate animals: Nothing to report.

6. PRODUCTS

Submitted Publication:

Comprehensive single and multiple, short and long-term pharmacokinetic studies of redox-active drug and SOD mimic, Mn(III) meso-tetrakis(N-butoxyethylpyridinium-2-yl)porphyrin, MnTnBuOE-2-PyP^{5+}
Artak Tovmasyan,[1] Tin Weitner,[1] Huaxin Sheng,[2] Xinghe Chen,[3] Kathleen Ashcraft,[1] Ping Fan,[4] Dewhirst, M. W.,[1] David S. Warner,[2] Zeljko Vujaskovic,[4] Ines Batinic-Haberle[1] and Ivan Spasojevic,[6]*

Departments of Radiation Oncology,[1] Anesthesiology, [2] Medicine,[6] and Duke Cancer Institute,[4] Duke University School of Medicine, Durham, NC 27710, Department of Neurosurgery, The First Hospital of Qinhuangdao City, Hebei, 066000 China,[3] and Division of Translational Radiation Sciences, Department of Radiation Oncology, University of Maryland, Baltimore, Maryland[5]

Presented Poster Presentation:

Application of the rat grimace scale to measure pain from cold allodynia. Lonnie E. Schneider, Katheryn Y. Henley, and Candace L. Floyd. Presented at the International Symposium on Neuronal Regeneration.

7. PARTICIPANTS & OTHER COLLABORATING ORGANIZATIONS

NAME	CANDACE FLOYD
PROJECT ROLE	PI
NEAREST PERSON MONTH WORKED	1.2
CONTRIBUTION	Project management, assessment of SCI in rodents
OTHER FUNDING SUPPORT	NIH, UAB, other DoD

NAME	HUBERT TSE, PH.D.
PROJECT ROLE	Co-PI
NEAREST PERSON MONTH WORKED	1.2
CONTRIBUTION	Assessment of cytokines and inflammation, data interpretation
OTHER FUNDING SUPPORT	NIH, UAB, American Diabetes Association

NAME	DAVID WARNER, M.D.
PROJECT ROLE	Co-PI
NEAREST PERSON MONTH WORKED	2.1
CONTRIBUTION	Subcontract project management and oversee the mouse SCI induction
OTHER FUNDING SUPPORT	DUKE

NAME	IVAN SPASOJEVICK, PH.D.
PROJECT ROLE	CO-I
NEAREST PERSON MONTH WORKED	1.2
CONTRIBUTION	Conduct and coordinating the pharmacokinetic assessments
OTHER FUNDING SUPPORT	DUKE

NAME	INES BATINIC-HABER, PH.D
PROJECT ROLE	CO-I
NEAREST PERSON MONTH WORKED	0.9
CONTRIBUTION	assess the purity of BuOE2, assist with data interpretation and PK
OTHER FUNDING SUPPORT	DUKE

NAME	XUZXIN SHENG, M.D.
PROJECT ROLE	3.0
NEAREST PERSON MONTH WORKED	CO-I
CONTRIBUTION	Assessment of ischemic SCI in mice
FUNDING SUPPORT	DUKE

NAME	LONNIE SCHNEIDER
PROJECT ROLE	TECHNICAL (POST-DOC)
NEAREST PERSON MONTH WORKED	12
CONTRIBUTION	Conduct experiments related to rat SCI
FUNDING SUPPORT	NONE

NAME	GARY MASSEY
PROJECT ROLE	TECHNICAL
NEAREST PERSON MONTH WORKED	1.2
CONTRIBUTION	Assist with induction and evaluation of SCI in mice
FUNDING SUPPORT	DUKE

NAME	ARTAK TOVMASYAN
PROJECT ROLE	TECHNICAL (POST-DOC)
NEAREST PERSON MONTH WORKED	1.8
CONTRIBUTION	Assist with PK evaluations
FUNDING SUPPORT	DUKE

8. QUAD CHART

SEE NEXT PAGE

9. APPENDIX 1 AND 2

SEE NEXT PAGES:
APPENDIX 1, SUBMITTED MANUSCRIPT
APPENDIX 2, RESEARCH POSTER

Comprehensive single and multiple, short and long-term pharmacokinetic studies of redox-active drug and SOD mimic, Mn(III) *meso*-tetrakis(*N*-butoxyethylpyridinium-2-yl)porphyrin, MnTnBuOE-2-PyP^{5+}

by

Artak Tovmasyan,[1] Tin Weitner,[1] Huaxin Sheng,[2] Xinghe Chen,[3] Kathleen Ashcraft,[1] Ping Fan,[4] Dewhirst, M. W.,[1] David S. Warner,[2] Zeljko Vujaskovic,[4] Ines Batinic-Haberle[1] and Ivan Spasojevic,[6]*

Departments of Radiation Oncology,[1] Anesthesiology, [2] Medicine,[6] and Duke Cancer Institute,[4] Duke University School of Medicine, Durham, NC 27710, Department of Neurosurgery, The First Hospital of Qinhuangdao City, Hebei, 066000 China,[3] and Division of Translational Radiation Sciences, Department of Radiation Oncology, University of Maryland, Baltimore, Maryland[5]

[*]Corresponding author

Ivan Spasojevic, PhD
Department of Medicine
PK/PD Duke Cancer Institute Shared Resource
Duke University School of Medicine, Durham, NC 27710
Tel: 919-684-8311
e-mail: ivan.spasojevic@duke.edu

Abstract

Cationic Mn(III) N-substituted pyridylporphyrins (MnP) have been optimized to increase their biodistribution and toxicity without compromising their redox-active properties. Most recent analog, MnTnBuOE-2-PyP^{5+}, has been synthesized and its therapeutic effects assessed. It possesses a high ability to catalyze O$_2$$^-$ dismutation (SOD-like activity) and peroxynitrite (ONOO$^-$) and hypochlorite (HClO$^-$) reduction, and impact cellular metabolism at least in part affecting cellular transcription activity. Its distribution and efficacies in central nervous system injuries and in mitochondria have been well-documented. Along with efficacy studies comprehensive pharmacokinetic (PK) studies were conducted to evidence its biodistribution and facilitate the proper dosing regime and identify preferred routes of administration. A single 72 h-PK mouse study was performed *via iv* and *sc* routes; the levels in plasma, liver, kidney, spleen, colon, heart, lung and brain were determined and PK parameters, AUC, $t_{1/2}$, C_{max} and t_{max} calculated. Highest levels were found in liver and kidney, followed by lung, heart and spleen, while the lower levels were demonstrated in colon and the lowest in brain. Further, a long-term 56-day single and multiple dosing PK study *via sc* route at 4 different concentrations of 0.5/kg, 1 mg/kg, 3 mg/g and 10 mg/kg, was conducted. MnP was given as **(i)** a single injection, **(ii)** once weekly and **(iii)** once every second week. The levels of MnP in liver, brain, spinal cord, salivary glands, and tongue were measured and PK parameters, AUC, $t_{1/2}$, C_{max} and t_{max} calculated. Finally, accumulation of MnP at one day, 7 and 28 days of twice-daily administration of 4 doses (0.5, 1.5, 4.5 and 9 mg/kg) was conducted. No saturation levels were reached at 28 days of such dosing. No change in mouse weight was observed at any dose. The accumulation of MnP in brain and spinal cord is slower than in other organs where the pharmacokinetics follows the liver profile. The oral availability of three lead MnPs, MnTE-2-PyP$^{5+,}$ MnTnHex-2-PyP^{5+} and MnTnBuOE-2-PyP^{5+}, was re-evaluated to be 0.6, 2.9 and 3.9%; it follows trend in their hydrophilicities, MnTE-2-PyP^{5+} being the most hydrophilic one. The mouse perfusion, prior to organ extraction has been a routine strategy to avoid the contribution of blood MnP levels in organ measurements. We have demonstrated herein that such approach is safe as it does not extract MnP from the tissue.

Introduction

MnTnBuOE-2-PyP^{5+} is an optimized cationic, fairly lipophilic Mn(III) N-butoxyethylpyridylporphyrin with favorable interplay of redox activities bioavailability and lipophilicity. Its redox properties are accurately described by its metal-centered reduction potential for Mn^{II}P/Mn^{II}P redox couple and ability to catalyze O$_2$$^-$ dismutation, log k_{cat}(O$_2$$^-$)]. It crosses blood brain barrier and accumulates in both brain and heart mitochondria [1, 2]. It is few fold less toxic than otherwise similarly lipophilic analog, MnTnHex-2-PyP^{5+} [3, 4]. Differences in the structure of pyridyl substituents between these two Mn porphyrins are not yet fully understood, but affect their bioavailibilities [3, 4]. Both compounds have 6 C atoms in their pyridyl substituents. Yet, MnTnBuOE-2-PyP^{5+} has one oxygen atom in each of four pyridyl substituents; subsequently it is slightly more hydrophilic that MnTnHex-2-PyP^{5+}. Its polar oxygen atoms with 2 electron pairs, each, seemingly affect its transport into mitochondria and retention in lipid membranes, brain included [1, 2].

Both compounds are under preclinical exploration *in vitro* and *in vivo*. MnTnBuOE-2-PyP[5+] has been firstly tested in an O_2^- specific *in vivo* model – aerobic growth of SOD-deficient yeast *Saccharomyces cerevisiae* where it allows this organism to grow as well as wild type [4, 5]. It has then been forwarded into other cellular and animal models as well as biodistribution studies. MnTnBuOE-2-PyP[5+] was shown to accumulate in brain and its parts [1-3, 6] and in brain and heart mitochondria [1, 2, 7]. The direct evidence was provided that MnTnBuOE-2-PyP[5+] mimics mitochondrial SOD isoform, MnSOD. The work was done on MnSOD over-expressor- and knock-out mice, where MnTnBuOE-2-PyP[5+] protects HaCaT human keratinocytes against UV radiation-induced oncogenic transformation *via* inside-out signaling [8]. MnTnBuOE-2-PyP[5+] also suppresses doxorubicin-induced mitochondrial dysfunction in neonatal rat heart cells H9C2 [8, 9] [Miriyala et al., submitted]. In a mouse model this MnP affords whole brain radioprotection [10, 11]. MnTnBuOE-2-PyP[5+] [10]10 and MnTnHex-2-PyP[5+] [3] acted as radio- and chemo-sensitizors in a D-245 MG glioblastoma sc mouse xenograft model. Further, in a mouse head and neck radioprotection model MnTnBuOE-2-PyP[5+] protects salivary glands [12], while in a head and neck tumor sc xenograft mouse study MnTnBuOE-2-PyP[5+] acted as radiosensitizer suppressing tumor growth [12]. In such scenario, MnP employs H_2O_2 to catalyze thiol oxidation of numerous proteins which results in tumor cell death [13-16]. The differential actions of MnP with respect to tumor (cytotoxic) and normal tissue (radioprotective), arising from their different redox environment, make MnPs prospective candidates as tumor radio- and chemo-therapeutics. Recently, instead of radiation, the MnP/ascorbate system was used as a ROS generator and promoted tumor death in cellular and animal studies [3, 17-19]. In a cellular lymphoma model, MnTnBuO-2-PyP[5+] and MnTE-2-PyP[5+] enhanced the anticancer effect of dexamethasone (Tome et al, unpublished) [13, 14]. Erectile dysfunction is a serious side effect of prostate radiation and greatly reduces willingness of patients to undergo such treatment. In a rat prostate radiation model, MnTnBuOE-2-PyP[5+] was able to greatly rescue erectile function in a similar fashion to the action of its analog, MnTE-2-PyP ([20], Oberley et al unpublished). We have further shown the potency of MnTnBuoE-2-PyP[5+] in suppressing chronic morphine tolerance in a mouse model under conditions previously reported for earlier analogs MnTE(or nHex)-2-PyP[5+] ([21] [Warner et al, unpublished]. MnTnBuOE-2-PyP[5+] exhibited remarkable ability to minimize itch in a mouse model [22] [Ji, Liu et al, unpublished]. Itch was induced *via* chloroquinone, which activates pruriceptors or compound 48/48. Compound 48/48, which promotes histamine release, is a polymer produced by the condensation of *N*-methyl-*p*-methoxyphenethylamine. MnTnBuOE-2-PyP[5+] increased survival and reduced long-term movement deficit in a galactose-1P uridylyltransferase-null mouse model of galactosemia [23]. Thus far, MnTnBuOE-2-PyP[5+] was tested in mice and rats at single and multiple dosing in the range of 0.1 to 3.2 mg/kg per day given daily or several times per week for up to 6 weeks *via* ip or *sc* routes. In cellular studies it was efficacious in a range of 0.1 to 20 μM, depending upon the type of a cell. **Figure 1** summarizes the *in vitro* and *in vivo* therapeutic effects of MnTnBuOE-2-PyP[5+] [1-12, 15].
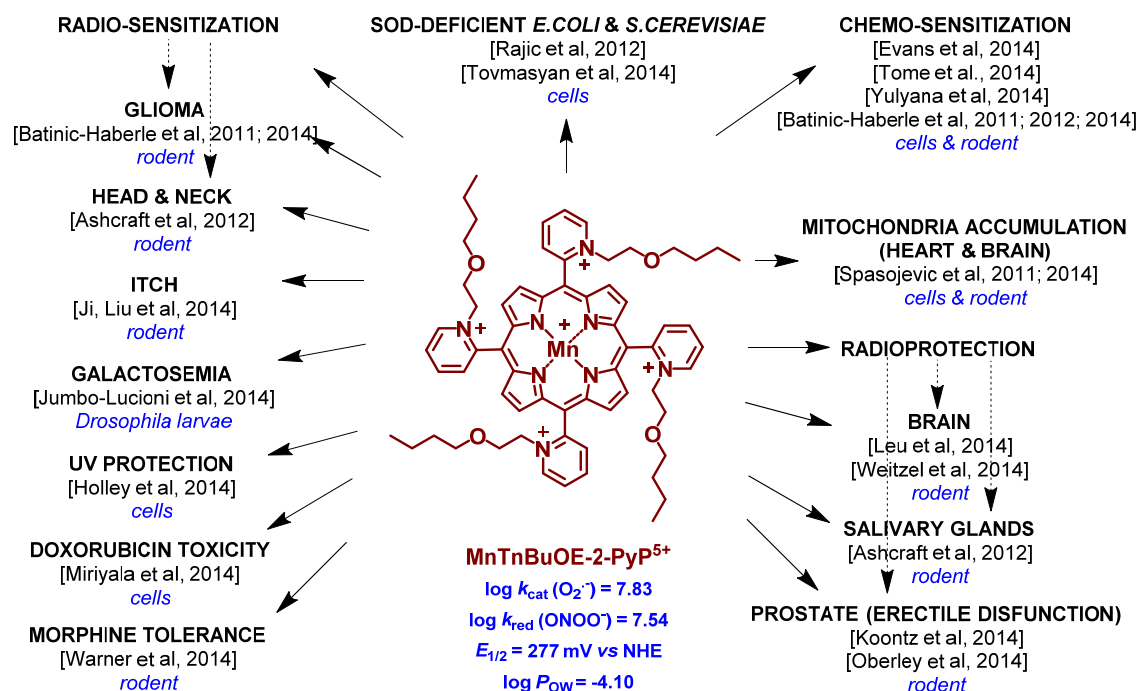
Figure 1. The *in vitro* and *in vivo* therapeutic effects of MnTnBuOE-2-PyP^{5+} (BMX-001). Also listed are: metal-centered reduction potential for Mn^{II}P/Mn^{II}P redox couple, $E_{1/2}$, the ability of MnP to catalyze O$_2^-$ dismutation, log k_{cat}O$_2^-$, the ability to reduce ONOO$^-$ and lipophilicity in terms of partition between n-octanol and water, log P_{OW}.

Artak, add subarachnoid hemorrhage as unpublished, add mucose at salivary glands" Salivary Glands & Mucose

The initial therapeutic effects observed have justified the subsequent comprehensive PK studies. We have herein determined the maximal tolerable single dose *via iv* and *sc* routes of administration. Subsequently we performed a single PK study *via sc* and *iv* routes and analyzed MnP in all major organs: liver, kidney, spleen, lung, heart, brain, spinal cord and colon. To account for the preclinical studies targeting brain and head and neck cancer and radioprotection we have assessed levels in brain, salivary glands and tongue also. Due to our interest in developing Mn porphyrins for the injuries of central nervous system, spinal cord was analyzed also. The 24-hour single injection PK study was followed with a long-term comprehensive 56-day multiple dosing PK study at 4 different concentrations. The goal was to provide the information on the frequency of dosing needed to maintain levels in organs high enough to assure therapeutic efficacy, *i.e.* avoid toxic.

The reports on PK studies of Mn porphyrins and drugs in general are rare, while essential for proper therapeutic effects [24] Moreover, usually only plasma PK profiles are reported, and very rarely organ levels (see references in [24].

Experimental

Porphyrins and other chemicals. MnTnBuOE-2-PyP^{5+} (λ_{max} = 454.0 nm, log ε = 5.14), and MnTnHep-2-PyP^{5+} (λ_{max} = 454.0 nm, log ε = 5.19) as a standard were synthesized and characterized as previously described [25, 26]. Other chemicals used were acetonitrile (MeCN) by Fisher Scientific, methanol (anhydrous, absolute) by Mallinckrodt, glacial acetic acid by EM Science, heptafluorobutyric acid (HFBA) by Aldrich and phosphate-buffered saline (50 mM sodium phosphate, 0.9% NaCl, pH7.4) by Gibco.

Mice. Duke University Medical Center Animal Facility has a continuously accredited program from AAALAC International. All experiments using animals were performed according to the approved protocol for humane care and use of animals. The 10-weeks old C57BL/6J female mice weighing 17-25 g were used.

Maximal tolerable dose. Firstly, the maximal tolerable dose was determined for *sc* and *iv* route by step-wise increasing the dosing with 3 mice per dose until significant impact on mouse behavior, such as quietness, reluctance to move some of those caused by acute blood pressure drop, was observed. A single *sc* dose of 10 mg/kg of MnTnBuOE-2-PyP^{5+} and *iv* dose of 2 mg/kg were identified as MTD. The concentration of aqueous solutions (for oral gavage) or saline solutions (for subcutaneous, sc and intravenous, iv injections) of MnTnBuOE2-PyP^{5+} was adjusted so that mice were injected with ~ 0.1 mL per dose.

Single dose 72h-PK study. In a single dose 72-h Pk study the *sc* and *iv* dosing were compared, the plasma and organ levels were analyzed at different time points within 72 h. For *iv* injections mice were anesthetized with isoflurane in 30% oxygen balanced with nitrogen and a PE-10 tubing was surgically implanted into right jugular vein. 0.1 ml BuOE2 solution was slowly infused using 1 ml syringe. Then the PE-10 tubing was removed and skin incision was closed. Mouse was returned into the cage after injection. For PK studies, mice were euthanized at different time points (5 min to 24 hours), with 3 mice per time point.

Long-term 56-day single and multiple dosing sc PK study. This study was conducted at 4 different doses of 0.5, 1, 3 and 10 m/kg, given *via sc* route. Analyses were done for: **(i)** single dosing at days 1, 3, 7, 14, 28 and 56 days; **(ii)** weekly dosing at 7, 14, 28, and 56 days; and **(iii)** every second week at 14, 28, and 56 days.

Long-term 7-day and 28-day PK study. MnTnBuOE-2-PyP^{5+} was given *sc* in two daily increments at 4 different doses of 0.5, 1.5, 4.5 and 9 mg/kg given for the duration of 1 day, 7 days and 28 days. Samples were taken as described below for tissue collection at 12 hours after the last injection. 13 groups of mice (including control group with no drug administration) with 3 mice per group were analyzed. 3 mice per group were analyzed.

Organ collection. In all studies mice were perfused prior to tissue collection. Exception was only a study where comparing perfusion vs non-perfusion method used in tissue collection was compared. The perfusion was conducted in following way. Mice were re-anesthetized with 5% isoflurane in 30% oxygen balanced with nitrogen. Then mice were intubated and mechanically controlled by a rodent ventilator (Harvard model 683) with the tidal volume of 0.7 ml and the rate of 105 strokes/minute. Isoflurane was reduced to 1.8% for subsequent procedure. The chest was open to explore the heart. 0.5 ml arterial blood was directly sampled from left ventricle. Then a blunt 20 gauge needle was inserted into aorta via left ventricle and a small cut was made on right atrium. The vasculature was

briefly rinsed with 60 mL saline by transcardial perfusion prior to excision of liver, kidney, spleen, lung, heart, and brain. Fresh blood mixed with heparin was centrifuged at 2500 rpm for 10 minutes. Plasma and hematocytes were separated immediately. Samples were kept at -80^0C.

MnP extraction from plasma and organs. Organs were cryo-pulverized in a Bessman tissue pulverizer (BioSpec Products, Bartlesville, OK) under liquid nitrogen and then homogenized in a rotary homogenizer (PTFE pestle and glass tube) with 2 volumes of deionized water. An aliquot of either plasma or tissue homogenate was transferred into a 2 mL polypropylene screw-cap vial and a double volume of 1% acetic acid in methanol was added and mixed by vortexing for 30 sec (1:2 homogenate:1% acetic acid). Samples were treated twice in the FastPrep apparatus (Qbiogene, Carlsbad, CA) at speed 6.5 for 20 sec and subsequently centrifuged 10 min at 13,000 g to separate proteins. An aliquot of the supernatant was pipetted into a 5 mL polypropylene tube (10×50 mm) and the solvent was completely removed in a Savant Speed-Vac evaporator at 40°C within 1 h. The dry residue was dissolved in a 20 μL of mobile phase B (see below) and sonicated for 5 min, then 80 μL of mobile phase B was added, the mixture was sonicated again for 5 min and centrifuged for 5 min at 4500 g at 4°C. Finally, the tube content was transferred to the HPLC autosampler polypropylene vial equipped with silicone/PTFE septum, followed by another cycle of centrifugation for 5 min at 4500 g (4°C), after which the sample was immediately analyzed by LC-MS/MS.

LC-MS/MS analysis of MnP levels in plasma and organs. Quantitative analysis was performed on a Shimadzu 20A series HPLC (LC) - Applied Biosystems MDS Sciex 3200 QTrap or 4000 QTrap tandem-mass spectrometer (MS/MS) at Pharmacology Laboratory (Shared Resource PK/PD and Small Molecule Analysis Core) of Duke Cancer Center. The use of HFBA as an ion-pairing agent increases overall lipophilicity/volatility and greatly improves retention and ionization efficiency of the analytes, affording an abundance of $[MnP^{5+} + 2HFBA^-]^{3+}$ and $[MnP^{5+} + 3HFBA^-]^{2+}$ ions. Solvents employed were: A = 95:5 H_2O:MeCN (0.1% HFBA); B = MeCN (0.1% HFBA). MnTnBuOE-2-PyP^{5+}, like all *ortho* Mn(III) *N*-substituted pyridylporphyrins, exists as a mixture of four atropoisomers. With the chosen solvent system all four atropoisomers of MnPs [27] collapsed into a single peak enhancing the sensitivity of the method to as low as 0.5 nM (nanomoles per mL of tissue homogenate). Analyses were performed using a Phenomenex Luna C18 guard cartridge (ID x L, 2 x 4 mm) only. Specific mass transitions m/z $[MnP^{5+} + 3HFBA^-]^{2+}$ to m/z $[MnP^{5+} - alkyl^+]$ fragmentation were followed: MnTnBuOE-2-PyP^{5+} at m/z = 857.3/599. For short 24-h PK study MnTnHep-2-PyP^{5+} was used as internal standard at m/z 853.5/639.5. For long term 56 day PK multi-dosing PK study, the deuterated, MnTnBuOE-2-PyP^{5+}-d_8 compound was used as internal standard with m/z = 862.2/603.9. Deuterated compound was obtained from Albany Molecular Research who GMP-scaled up the compound. Calibration samples in 1–300 nM or 0.1–30 μM range (depending on the expected levels of MnP) were prepared by adding known amounts of serially diluted pure standards into homogenates of the corresponding tissues and were analyzed along with study samples. Response was calculated as the ratio between the standard peak area and internal standard peak area. The extraction of a lipophilic MnTnBuOE-2-PyP^{5+} and the preparation of the plasma and tissue samples for analysis has been further improved in this study. Relative to

hydrophilic MnTE-2-PyP^{5+}, the analysis of lipophilic MnPs is more challenging due to their affinity for proteins and plastic and glass surfaces. Thus, each MnP needs specific method adjustments as well as different internal standard.

Re-evaluation of oral availability. We have reported that cationic Mn(III) *N*-alkylpyridylporphyrins (MnTE(or nHex)-2-PyP^{5+}) are ~ 20% orally available [24]. We have subsequently performed, in a same manner as with MnTE(or nHex)-2-PyP^{5+}, a single-dose 72-h oral availability PK study for alkoxyalkyl analog, MnTnBuOE-2-PyP^{5+} [1-3, 24, 28]. When we subsequently tried to assess the outcome of a long-term oral administration of MnTnBuOE-2-PyP^{5+} *via* drinking water, no significant MnP levels in plasma and liver were found; no aversion of mice to drinking was observed as expected daily amount of water per mouse was consumed. Another long-term comprehensive study with MnTnHex-2-PyP^{5+} followed. Doses as high as 2 and 5 mg/kg/day were given *via* oral gavage. MnTnHex-2-PyP^{5+} was given daily for **(i)** one week; **(ii)** two weeks; **(iii)** three weeks, and **(iv)** 4 weeks. MnP levels in liver were determined with all 4 dosing regims at **(a)** 2 hours; **(b)** 6 hours, and **(c)** 24 hours post last oral gavage. When 5 mg/kg MnP was given for a week, the liver levels at 24 hours after oral gavage (where no contribution of plasma levels to MnP organ levels were expected as mice were perfused) were low, ~ 36 to 78 nM; the expected values were projected based on earlier study to be well above 4,454 nM. For the sake of precision in collecting plasma and organs during early time points, we gave drug orally directly into the stomach of anesthetized mouse in a following way. The 7-8 cm blunt polyethylene tubing PE-50 tube was connected to a 1 ml syringe. Tubing was marked 5 cm from the tip to know when it reaches stomach. Mouse was anesthetized in the chamber containing 5% isoflurane in 30% oxygen balanced with nitrogen. The PE 50 tube was gently inserted into esophagus and advanced into stomach along the left wall of mouth. The tube was advanced until the mark on the tube reaches nose of the mouse. The 0.1 ml of compound was infused. Then the tube was slowly withdrawn. It appeared that such strategy might have allowed for a reflux into the respiratory pathways. At alter time points beyond 2 h drug was give into the mouth cavity of awaken mouse.

We were for a while puzzled with large scattering of the data within early time period of a PK profile for all three MnPs, MnTE(or nHex or nBuOE)-2-PyP^{5+} [24]. We had initially attributed such scattering to the differences in the oral absorption among individual mice. Yet, it was not before we failed to detect MnP in a liver in a long-term oral gavage study, that we reconsidered the scattering of the data within early time points. The only difference between the early and later time points was in the way how we administered drug orally: into the stomach *vs* mouth cavity. We believed that our strategy of giving drug directly into the stomach of anesthetized mouse was a precise approach in collecting blood and organs at very early time points. Reflux was not anticipated as it was commonly assumed that any entrance of a drug into respiratory system would cause huge distress or even death of a mouse. While anesthetized during drug delivery, mice were in horizontal position supplied with artificial breathing. *All 3 conditions combined - anesthesia, horizontal position and artificial breathing - allowed for the reflux of a drug into the respiratory system and subsequently into the plasma and accounted for ~20% of intravenous levels.*

To prove such hypothesis, we designed a study depicted in **Table 1**. In addition to traditional oral gavage into the mouth cavity, we administered MnTnHex-2-PyP^{5+} directly into the respiratory system, at 20% and 10% of the total 2 mg/kg dose given into the mouth or stomach. We kept the mouse anesthetized either with or without artificial breathing through 2 h-duration of the study. We also had a group of mice where no anesthesia was applied

(groups 3 and 6). We also have a group of mice where we injected drug directly into intestine to account for possible intestine availability only. In another group of mice, we sutured the stomach to prevent MnP availability *via* intestine. MnP reaches C_{max} in plasma very fast, for *sc* route it was found to be ~ 1hour. Thus, the plasma MnP levels were determined at 10 min and 2 hours. No significant absorption of MnP *via* stomach or intestine was demonstrated. The 100% of a drug given into oral cavity of non-anesthetized mouse without artificial breathing does not reach plasma at any significant level. Artificial breathing greatly enhanced reflux: 20% of 2 mg/kg given into the mouth of anesthetized mouse with artificial breathing reaches blood at significantly higher levels (**Figure 1**). When 10% of the total drug was given into trachea of a mouse under artificial breathing the amount found in plasma of ~113 nM at 10 min post-injection was 5-fold higher than when 100% of a dose was given into the mouth of awaken mouth (24 nM) (compare groups 3 and 6 in **Figure 1**). The 113 nM levels which presents the 10% availability of 2 mg/kg dose *via* trachea agree well with data we reported on oral availability achieved within first minutes post administration reported [24]. The assumption is here made that the whole amount of MnP which enters trachea reaches the blood. We then recalculated the oral availability accounting for the period 2 h to 24 h only when the drug was given *via* oral gavage into the mouth (**Figure 2**). It was found to be 2.9% (**Figure 2**). The oral availability of MnTnBuOE-2-PyP^{5+} was initially calculated in the same way as MnTnHex-2-PyP^{5+} and with MnTE-2-PyP^{5+} to be ~20% [3, 24] (**Figure 2B**). It was then recalculated here to be 3.9% (**Figure 2A&C**). The 0.6% oral availability of MnTE-2-PyP^{5+} was recalculated in the same way (**Figure 2A&C**) in agreement with more hydrophilic nature of this porphyrin. Our re-assessment of the oral availability of cationic Mn porphyrins agree with the outcome of efficacy study published by Salvemini's group where the lack of the protective effect of MnTE-2-PyP^{5+} in carrageenan-induced hyperalgesia was demonstrated when it was given *orally*, but not *ip* [29].

Table 1. Re-evaluation of the MnP oral availability. The study was designed to provide evidence that the drug reflux into respiratory system during oral gavage experiment accounted for high blood and organ oral availability. MnTnHex-2-PyP^{5+} was given to anesthetized mouse with and without artificial breathing, and was analyzed in plasma at 10 min (shown below) and 2 hours. Different ways of administration were herein explored to differentiate the drug access to blood: *via* oral GI tracts or *via* respiratory system.

Group	Delivered	Inhalation Anesthesia (isoflurane)	Comments
1	Intestine (100% dose)	yes	Sutured towards stomach
2	Stomach (100% dose)	yes	Sutured towards intestines and esophagus
3	Oral cavity (100% dose)	no	With a OG needle (slow delivery)
4	Oral cavity (20% dose)	yes	20 uL
5	Trachea (10% dose)	yes	By PE10 tubing
6	Trachea (10% dose)	no	By PE10 tubing

A 2014-05-24 MnTE-2-PyP vs MnTnHex-2-PyP, vs MnTnBuOE-2PyP ORAL vs. IV/IP AUCs 2-24h after dosing

B MnP plasma concentration - ORAL (0-24h after dosing)

C

dosing	AUC (2-24h) / µM h		
	MnEt	MnHex	MnBuOE
IV	6.23 ± 0.04	-	
IP	-	4.6 ± 0.2	2.5 ± 0.1
ORAL	0.038 ± 0.002	0.14 ± 0.01	0.19 ± 0.01
F=	0.6%	2.9%	3.9%
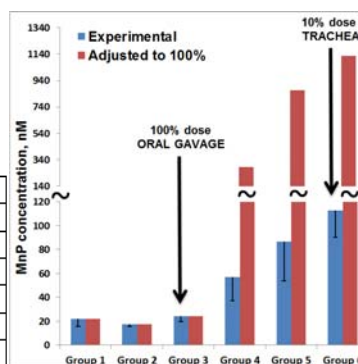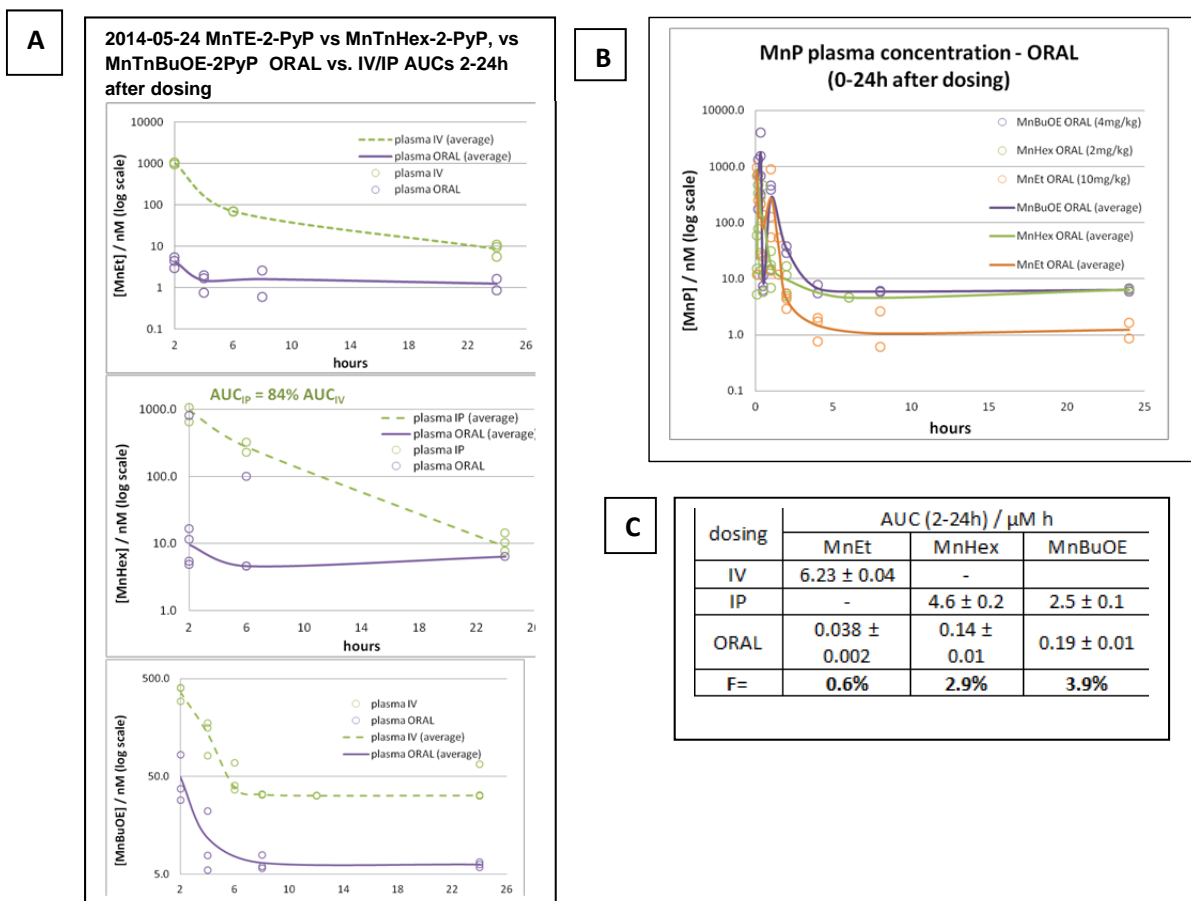
Figure 2. The re-evaluation of the oral availability of lipophilic Mn porphyrins, MnTE-2-PyP[5+], MnTnHex-2-PyP[5+] and MnTnBuOE-2-PyP[5+]. **(A)** PK profiles of all 3 Mn porphyrins when given into the mouse cavity *via* oral gavage for a period of 2-24 h; **(B)** The PK profiles for all 3 MnPs for the period of 0-24 h. During early time points MnP was given *via* polyethylene tubing into the stomach. As mouse was anesthetized and supplied *via* artificial breathing, some of the drug entered respiratory system and in turn blood and artificially increased blood MnP levels. **(C)** Recalculated data accounting only for 2-24 h period of time when MnP was given into mouth cavity of awaken mouse and when no significant scattering of data was observed [24]. The 2.9% of oral availability was obtained for MnTnHex-2-PyP[5+] which agrees well with the study conducted herein and laid out in **Table 1**. The similar, 3.9% oral availability was obtained for MnTnBuOE-2-PyP[5+]. As anticipated, few fold lower oral availability of 0.6% of MnTE-2-PyP[5+] was obtained for the most hydrophilic compound among three MnPs studied.

Evaluation of the perfusion vs non-perfusion strategy in extracting plasma and organs while assessing MnP PK profile.

Herein we analyzed the mice liver MnTnHex-2-PyP[5+] levels at 7 days after 10 mg/kg sc injection. 12 mice were distributed in 3 groups, 4 mice per group: **(i)** non-perfused; **(ii)** perfused either 30 mL; **(iii)** perfused with 60 mL saline. Perfusion was performed as described under MnP plasma/tissue extraction. The data are relevant to MnTnBuOE-2-PyP[5+] which has similar biodistribution. In all 3 groups of mice the levels found in plasma at 7 days after 10 mg/kg sc injections were essentially identical.
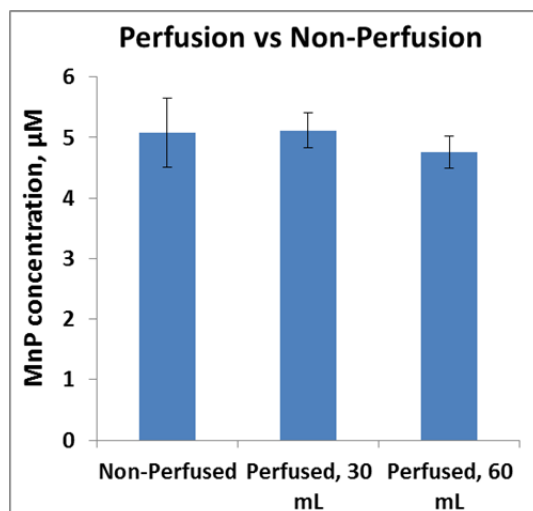
Figure 3. Evaluation of the impact of mouse perfusion prior to organ collection on the organ levels of MnTnHex-2-PyP⁵⁺. The livers of mice were analyzed at 7 days after *sc* 10 mg/kg single injection. 4 mice were analyzed per group. The data show that perfusion with 30 mL or 60 mL of saline did not reduce levels of MnP in organs.

Results and Discussion

The pharmacokinetic profiles are essential for the proper dosing of a drug in order to achieve the maximal therapeutic efficacy. Therefore single *sc* and *iv* 24-hour, and multiple long-term single injection, daily, weekly, and every second week, over 28 and 56 days (8 weeks), at 4 different doses PK studies were conducted to account for the biodistribution and clearances of MnP from target organs when drug was given for a long period of time.

Single dose 7-day sc and iv pharmacokinetic study. The single dose PK study was conducted with 10 mg/kg *sc* and 2 mg/kg *iv* injections identified as MTD. The PK curves are shown for several major organs in **Figure 4.** All data are provided in *Supplemental Material,* Figure 1S.
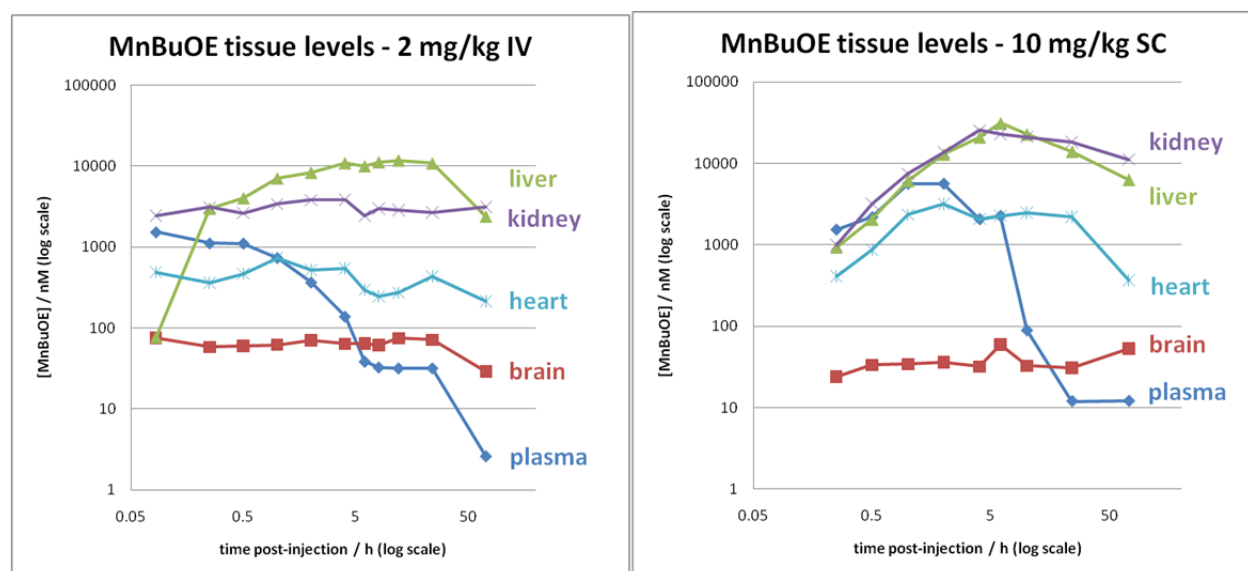
Figure 4. The 72-hour single dose plasma and organ *sc* and *iv* PK profiles of MnTnBuOE-2-PyP^{5+}. MnTnBuOE-2-PyP^{5+} was given *sc* at 10 mg/kg or *iv* at 2 mg/kg. The levels are given in nanomoles per 1000 mL of plasma or tissue homogenates. Time post-injection on x-axis is presented in log scale.

Non-compartmental analysis (WinNonlin; Pharsight, Inc.) was used to calculate the pharmacokinetic parameters given in **Table 2**. The biodistribution of MnTBuOE-2-PyP^{5+} in organs *via sc* relative to *iv* route of administration was given in **Figure 5**. Plasma drug body exposure was higher with *sc* then with *iv* route due to the higher clearance of MnP from plasma *via iv* route. As our earlier data on MnTE-2-PyP^{5+} and MnTnHex-2-PyP^{5+} show [24, 30, 31], the lowest availibility of this class of compounds was found in brain at 24 hours. Yet the long term 56-day PK study (see below) indicates that the MnP accumulation continues in brain during 10 days. The data In Figure 4 show that as MnP cleares from plasma, it continues to accumulate in all organs. Liver, kidney and spleen seve as reservoirs for the MnP accumulation and maintainance in other organs.

Table 2. **The 72-hour single dose *sc* and *iv* pharmacokinetic parameters of MnTnBuOE-2-PyP^{5+} for plasma and all organs**. MnTnBuOE-2-PyP^{5+} was given *sc* at 10 mg/kg or *iv* at 2 mg/kg. The AUC, C_{max}, t_{max} and clearance, $t_{1/2}$ (where a level decline was observed in the period 24-72 hours), were calculated.

Parameter→	AUC (µM h)					C_{max} (µM)				t_{max} (h)				$t_{1/2}$ (h)			
Sample ↓	IV	sd	SC	sd	F (%)	IV	sd	SC	sd	IV	sd	SC	sd	IV	sd	SC	sd
plasma	3.40	0.04	23.58	0.33	139	1.5	0.1	6.2	0.3	0.1	0.1	1.3	0.6	31	1	-	-
brain	3.91	0.02	2.82	0.02	14	0.083	0.002	0.06	0.01	4.1	6.9	28.0	38.1	85	8	-	-
liver	520.4	5.1	926.1	9.2	36	13.1	1.2	27.6	6.5	7.3	1.2	5.3	1.2	51	2	97	9
kidney	209.1	1.5	1160.4	14.9	111	4.1	0.4	29.1	2.4	2.0	1.7	5.3	1.2	-	-	158	33
spleen	60.5	0.5	115.8	8.1	38	1.7	0.3	2.2	0.3	13.3	9.2	28.0	38.1	58	4	-	-
lung	20.5	0.6	93.0	1.2	91	1.3	0.2	6.6	0.5	0.9	0.9	1.3	0.6	-	-	168	126
heart	23.7	0.7	103.0	1.4	87	0.76	0.15	3.2	0.6	2.0	1.7	9.3	12.7	124	71	43	3
colon	12.3	0.1	27.7	0.1	45	0.61	0.09	1.1	0.4	0.2	0.1	2.7	2.9	-	-	-	-
tongue	-	-	16.7	0.1	-	-	-	0.6	0.1	-	-	2.7	2.9	-	-	-	-
salivary gland	-	-	9.5	0.2	-	-	-	0.3	0.1	-	-	4.3	2.9	-	-	183	34
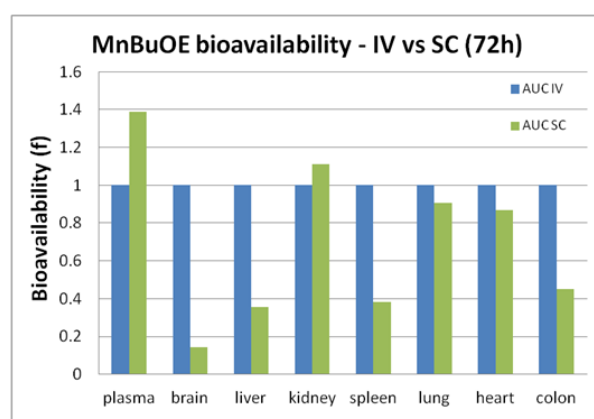
Figure 5. The 72-hour plasma and organ *sc* availability of MnTnBuOE-2-PyP^{5+} expressed relative to *iv* route.
The values determined *via iv* route are taken as 100 % availability. Single injections of MnTnBuOE-2-PyP^{5+} were given *sc* at 10 mg/kg or *iv* at 2 mg/kg. Bioavailability after sc administration (*f*, or *F* when expressed as %) is defined as a ratio, AUC$_{sc}$/AUC$_{iv}$, normalized by dose, according to the equation: $f = 100 \times [(AUC_{sc} \times dose_{iv})/(AUC_{iv} \times dose_{sc})]$. AUC values relate to 72-hour period.

Multi-dosing long-term 56-day sc pharmacokinetic study. MnTnBuOE-2-PyP^{5+} was given as **(i)** a single injection **(ii)** once a week and **(iii)** every second week and at 4 doses of (a) 0.5 mg/kg; **(b)** 1 mg/kg**; (c)** 3 mg/kg and **(d)** 10 mg/kg. Drug levels were followed for 8 weeks, 56 days; frequency of analysis of MnP levels in plasma and organs is shown in **Figure 5**. The plasma was collected at 6 time points, while organs were analyzed at 2, 4 and 8 weeks. The PK curves are provided in **Figure 6** and the PK parameters calculated in **Table 3**.
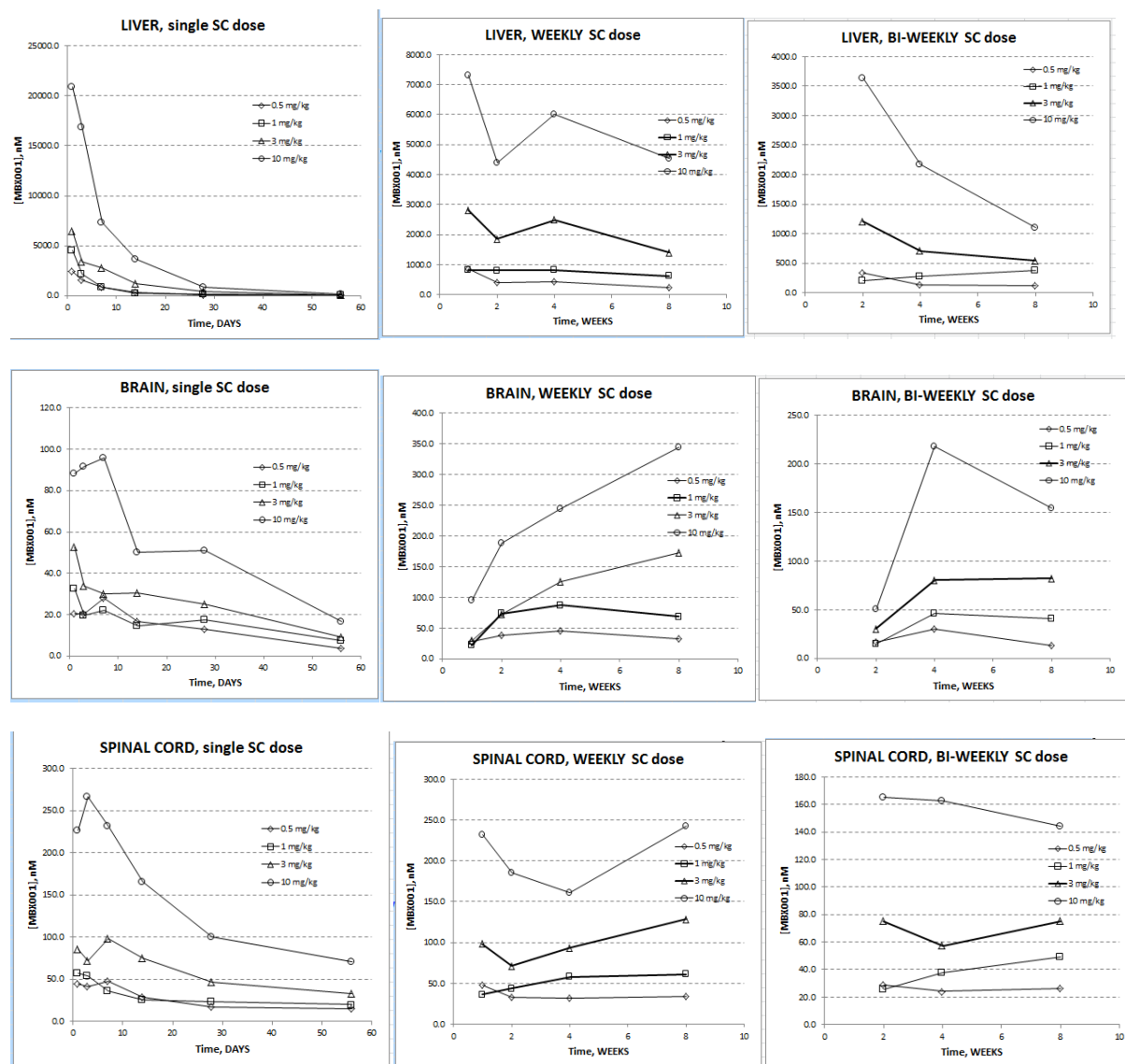
Figure 6. **The comprehensive** *sc* **PK study of MnTnBuOE-2-PyP^{5+}.** The MnP was given as a **(i)** single injection; **(ii)** once weekly; and **(iii)** once every second week (bi-weekly) and at several different doses: 0.5, 1, 3 and 10 mg/kg. MnP levels determined in plasma and in several organs at different time points. The organs to be analyzed were chosen in a way to cover studies where Mn porphyrins are explored in preclinical investigations (head and neck and brain tumors and central nervous system injuries). The PK data on salivary glands and tongue are provided in *Supplemental Material*, Figure S2.

Table 3. **The non-compartmental analysis of PK parameters for a single long-term 56 day *sc* PK study of MnTnBuOE-2-PyP^{5+}.**

Organ	Dose, mg/kg	AUC (1-56 days), day*μg/g	C_{max} (ng/g tissue)	t_{max} (days)	$t_{1/2}$ (28-56 day; d)	C at 56th day, ng/g tissue
Liver	**0.5**	22.9	3008	1	27	41
	1	29.2	5653	1	16	50
	3	71.4	8073	1	10	76
	10	226.5	26199	1	9	143
Brain	**0.5**	0.9	35	7	15	4
	1	1.1	41	1	23	10

	3	1.7	66	1	19	11
	10	3.5	120	7	17	21
Spinal cord	**0.5**	1.7	60	7	113	18
	1	1.8	71	1	120	25
	3	3.9	123	7	56	42
	10	9.1	333	3	54	88
Salivary gland	**0.5**	1.5	67	1	140	17
	1	1.7	132	1	107	19
	3	3.5	296	1	42	25
	10	9.6	817	1	27	48
Tongue	**0.5**	1.9	75	1	153	24
	1	2.2	108	1	100	26
	3	3.8	256	1	34	28
	10	8.3	573	1	25	37

The plasma and organ half-life, $t_{1/2}$, as well as AUC for 0.5 mg/kg *sc* 56-day dosing are shown in **Figure 7**. The highest availability was found in liver which serves as a drug reservoir to maintain stable levels of drug in other organs. We have chosen to concentrate on ≤ 1 mg/kg doses either given daily or every second day. Such doses are away from the multiple toxic doses which have been estimated for non-human primates in preliminary studies to be ≤ 6 mg/kg/day for 28 days. For comparison purposes the MnP distribution in different organs, in terms of AUC and $t_{1/2}$, are plotted in **Figure 7**. The values relate to 0.5 mg/kg 56-day single sc PK study. Based on $t_{1/2}$, the once-per-week dosing would maintain the stable MnP levels in organs.
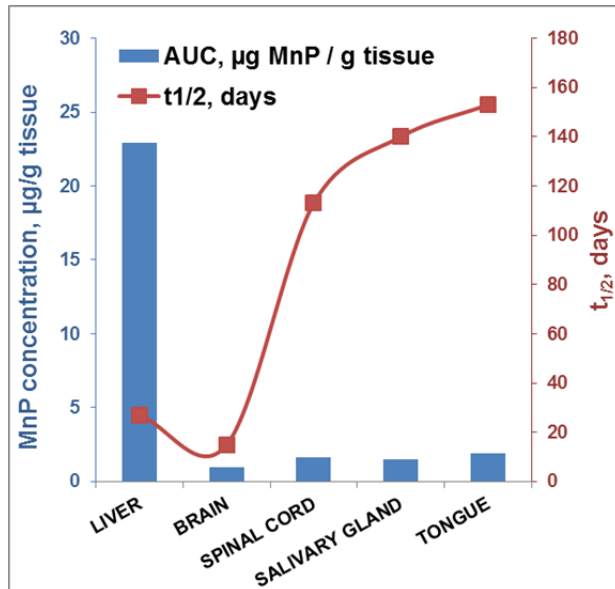
Figure 7. **The plasma and organ half-life, $t_{1/2}$, as well as AUC for 0.5 mg/kg *sc* 56-day single injection PK study of MnTnBuOE-2-PyP^{5+}**

Multi-dosing long-term 7-day and 28-day PK study. As compared to the 56-day PK study this study involved daily dosing over 7 and 28 days. Single dosing was conducted also. Mice were treated with single injection

at 4 different doses twice per day and for 7 and 28 days also. No loss in weight was demonstrated with all dosing schedules (Ashcraft et al, unpublished). Samples were taken at 12 hours after last injection to avoid the interference with high blood organ levels. The data related to plasma, liver and kidneys are shown in **Figure 8.** The data on other organs are shown in *Supplementary Material*. There is a constant accumulation of drug in all organs and saturation levels were not reached in any of the tissue analyzed.
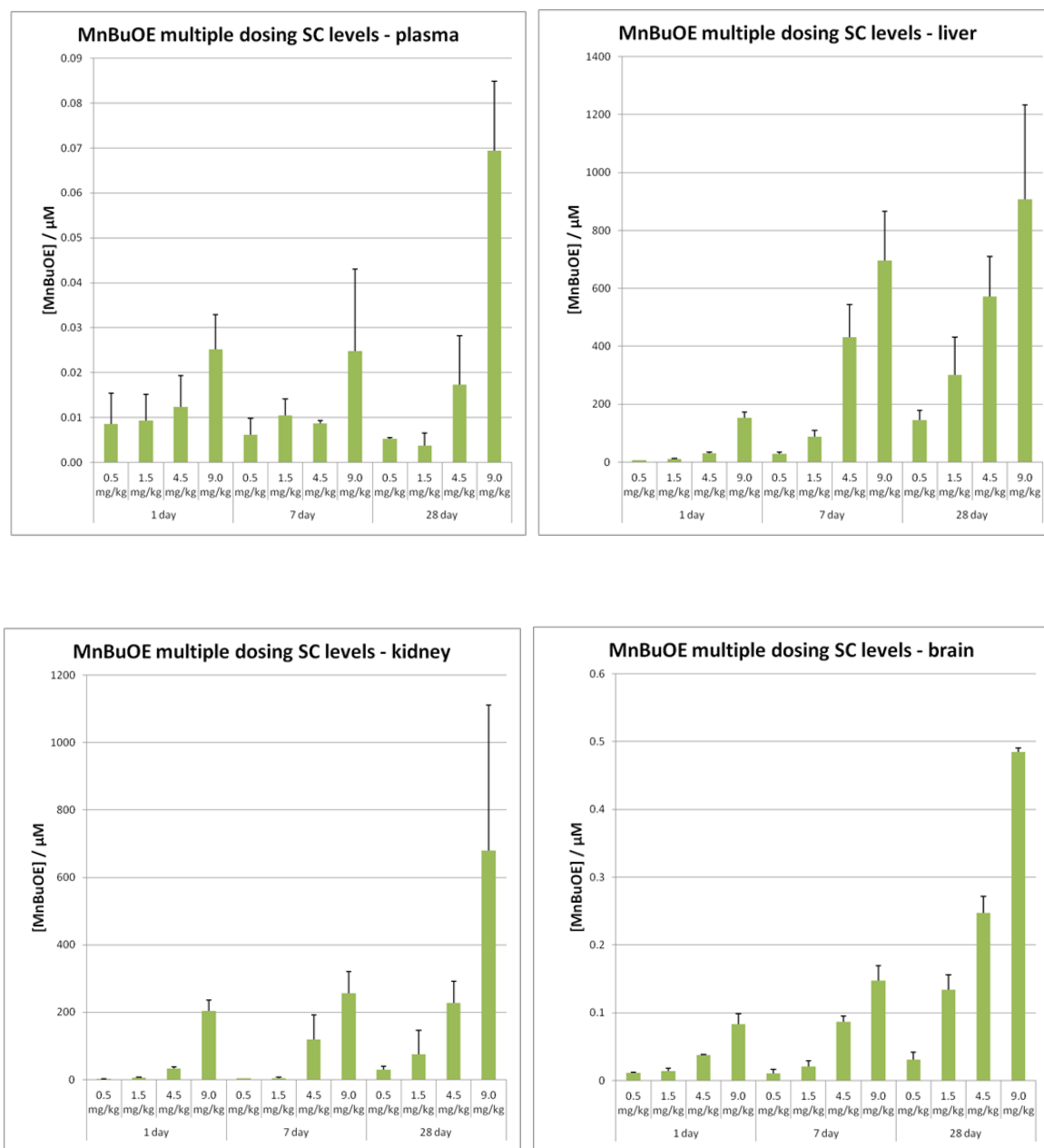
Figure 8. The accumulation of MnTnBuOE-2-PyP^{5+} in different organs after single injection (1 day), 7 days and 28 days dosing at 4 different doses given sc twice daily: 0.5, 1.5, 4.5 and 9 mg/kg. The samples were taken at 12 hours after last injection to minimize interference of the blood MnP with organ MnP levels. The MnP levels in plasma, liver, kidney and brain are given in micromoles per 1000mL plasma or tissue homogenate.

Reassessment of the oral availability of cationic Mn(III) N-substituted pyridylporphyrins. While experimental conditions were adjusted for the highest accuracy and precision, the possible significant impact of reflux in anesthetized mice supplied with artificial breathing onto MnP blood levels was overlooked when assessing MnP oral availiability. Consequently oral availability of cationic Mn(III) *N*-alkyl- and *N*-alkoxyalkylpyridylporphyrins was overestimated. We have here revisited their oral avilibility after failing to find the anticipated levels of Mn porphyrins when given either *via* oral gavage into the mouth cavity of awaken mouse, or as drinking water. The re-evaluation of the data sets oral avaibility of all 3 MnPs at ≥4%. The lowest value of 0.6% was found for most hydrophilic analog, MnTE-2-PyP^{5+}. However, our study opens the door to another excellent and facile route of their administration – inhalation. This exploration of this route of administration is particularly pertinent to the treatment of lung diseases.

Assessment of mouse perfusion prior to organ collection. We have routinely performed PK studies of MnPs in both plasma and organs. Thus far we have always perfused mice to assure that we have no contribution of plasma MnP's levels in their organ levels. This is particularly important when the levels of MnP in organs are assessed during first minutes up to 8 hours when MnP levels in plasma are still high. The issue, not earlier addressed, related to the possibility that perfusion forcefully clears the drug from intra- and extracellular space.

The perfusion vs non-perfusion experiment (**Figure 3)** was conducted at 7 day-time point. Relative to early time points, when MnP is still crossing the membranes and may localize to higher extent on the vessel walls, the MnP appears to be tightly bound inside cells/organs at day 7 post-injection. At that time point the perfusion does not affect levels of MnP as levels in plasma are lower than the lowest levels in organs. It is thus a safe strategy for anybody conducting PK studies to take organs at least 8 to 12 hours after last injection when levels in plasma are already low enough not to significantly affect organ levels and when MnP is presumably already within organs/cell and not on vessel walls.

At very early time points < 1 h, when plasma level are in high μM, and even though the mice were perfused, the data related to the organs (such as brain, **Figure 4**) with very low nM levels of porphyrins may be overstated and should be accounted for with caution.

Dosing of Mn porphyrins in preclinical studies. Appropriate dosing is crucial for the efficacy of any drug. Thus PK studies are essential to achieve maximal drug efficacy without compromising safety of animals and eventually humans. We have therefore conducted comprehensive PK studies herein and elsewhere in different animals and under different conditions [24, 28, 30, 32]. Based on such studies, it is obvious that Mn porphyrins exhibit a relatively slow clearance from all organs which allows for less frequent and patient-conveniently, once or twice weekly dosing, depending upon the targeted tissue. In most cases/organs one day is needed for MnP to peak;

thus whenever possible, the dosing should start at least 24 h before the oxidative-based injury. Different past and ongoing studies done on cells and animals [4, 10, 21, 33-35] suggest that more lipophilic drugs such as MnTnBuOE-2-PyP^{5+} and MnT nHex-2-PyP^{5+} are efficacious when administered at very low levels in the range of 0.1 to 1 mg/kg. The less lipophilic drugs, such MnTE-2-PyP^{5+} (and its methyl *ortho* and methyl and ethyl *meta* analogs) should be dosed at concentrations ≥5 mg/kg. The safety/toxicity profiles of MnPs are very much dependent upon their lipophilicities/accumulation which differ several orders of magnitude going from MnTM-2-PyP^{5+} over MnTnHex-2-PyP^{5+} to MnTnBuOe-2-PyP^{5+} [4, 5, 33, 36]. Based on our accumulation and mechanistic studies [5, 37] the more lipophilic compounds incorporate to a higher extent within membranes where they compromise their integrity. In addition their redox-properties play a role as non-redox-active Zn analogs are not toxic though they incorporate in membranes to similar levels driven by the nature of alkyl substituents on pyridyl nitrogens [3, 37-39]. With certain conditions, such as stroke, where fast accumulation in brain is required, *iv* route may be preferred. However, Mn porphyrins cause significant dose-dependent blood pressure drop (BPD) when given *via iv* route, and more so lipophilic analogs [40]. Therefore, *sc* route of administration (where BPD was much less expressed), though inferior with regards to the speed of CNS system delivery, is preferred whenever possible, as it still affords fairly fast delivery of MnP into all organs, and a large body exposure to MnP, AUC.

Acknowledgement

Abbreviations

$E_{1/2}$, half-wave reduction potential; SOD, superoxide dismutase; $k_{cat}(O_2^{-})$, rate constant for the catalysis of O_2^{-} dismutation by MnP; NHE, normal hydrogen electrode; P_{OW}, partition coefficient between n-octanol and water; $ONOO^{-}$, peroxynitrite; $O_2^{\bullet-}$, superoxide; ClO^{-}, deprotonated hypochlorite; MnTE-2-PyP^{5+}, AEOL10113, Mn(III) *meso*-tetrakis(*N*-ethylpyridinum-2-yl)porphyrin; MnTnHex-2-PyP^{5+}, Mn(III) *meso*-tetrakis(*N*-n-hexylpyridinum-2-yl)porphyrin; MnTnBuOE-2-PyP^{5+}, Mn(III) *meso*-tetrakis(*N*-n-butoxyethyllpyridinum-2-yl)porphyrin, BMX-001; PK, pharmacokinetics, AUC, are under curve; $t_{1/2}$, half-life; C_{max}, maximal concentration; C_{24}, concentration at 24 h; *ip*, intraperitoneal; *iv*, intravenous; *sc*; subcutaneous.

References

[1]   Spasojevic, I.; Miryala, S.; Tovmasyan, A.; Salvemini, D.; Vujaskovic, Z.; Batinic-Haberle, I.; St. Clair, D. Lipophilicity of Mn(III) *N*-alkylpyridylporphyrins dominates their accumulation within mitochondria and therefore *in vivo* efficacy. A mouse study. *Free Radic Biol Med* **51:**S98; 2011.

[2]   Spasojevic, I.; Weitner, T.; Tovmasyan, A.; Sheng, H.; Miriyala, S.; Leu, D.; Rajic, Z.; Warner, D. S.; Clair, D. K.; Huang, T. T.; Batinic-Haberle, I. Pharmacokinetics, Brain Hippocampus and Cortex, and Mitochondrial Accumulation of a New Generation of Lipophilic Redox-Active Therapeutic, Mn(III) *Meso* Tetrakis(*N*-n-butoxyethylpyridinium-2-yl)porphyrin, MnTnBuOE-2-PyP^{5+}, in Comparison with its Ethyl and N-hexyl Analogs, MnTE-2-PyP^{5+} and MnTnHex-2-PyP^{5+}. *Free Rad Biol Med* **65:**S132; 2013.

[3]   Batinic-Haberle, I.; Tovmasyan, A.; Roberts, E. R.; Vujaskovic, Z.; Leong, K. W.; Spasojevic, I. SOD Therapeutics: Latest Insights into Their Structure-Activity Relationships and Impact on the Cellular Redox-Based Signaling Pathways. *Antioxid Redox Signal* **20:**2372-2415; 2014.

[4]   Rajic, Z.; Tovmasyan, A.; Spasojevic, I.; Sheng, H.; Lu, M.; Li, A. M.; Gralla, E. B.; Warner, D. S.; Benov, L.; Batinic-Haberle, I. A new SOD mimic, Mn(III) ortho N-butoxyethylpyridylporphyrin, combines superb potency and lipophilicity with low toxicity. *Free Radic Biol Med* **52:**1828-1834; 2012.

[5]   Tovmasyan, A.; Reboucas, J. S.; Benov, L. Simple biological systems for assessing the activity of superoxide dismutase mimics. *Antioxid Redox Signal* **20:**2416-2436; 2014.

[6]   Weitzel D, A. K., Liu C, Li W, Buckley A, Rodriguiz RM, Wetsel WC, Spasojevic I, Tovmasyan A, Peters KB, Batinic-Haberle I, Dewhirst MW. Radioprotection of brain white matter by the catalytic MnSOD mimic / antioxidant, BMX-001. *Pediatric Neuro-Oncology Basic and Translational Research Conference*. Ft. Lauderdale, Florida; 2013.

[7]   Miriyala, S.; Spasojevic, I.; Tovmasyan, A.; Salvemini, D.; Vujaskovic, Z.; St Clair, D.; Batinic-Haberle, I. Manganese superoxide dismutase, MnSOD and its mimics. *Biochim Biophys Acta* **1822:**794-814; 2012.

[8]   Holley, A. K.; Xu, Y.; Noel, T.; Bakthavatchalu, V.; Batinic-Haberle, I.; St Clair, D. K. Manganese Superoxide Dismutase-Mediated Inside-Out Signaling In HaCaT Human Keratinocytes and SKH-1 Mouse Skin. *Antioxid Redox Signal*; 2014.

[9]   Zhao, Y.; Miriyala, S.; Miao, L.; Mitov, M.; Schnell, D.; Dhar, S. K.; Cai, J.; Klein, J. B.; Sultana, R.; Butterfield, D. A.; Vore, M.; Batinic-Haberle, I.; Bondada, S.; St. Clair, D. K. Redox Proteomic identification of HNE-bound mitochondrial proteins in cardiac tissues reveals a systemic effect on energy metabolism after Doxorubicin treatment. *Free Radic Biol Med* **In revision**; 2014.

[10]   Weitzel, D. H.; Tovmasyan, A.; Ashcraft, K. A.; Rajic, Z.; Weitner, T.; Liu, C.; Li, W.; Buckley, A. F.; Prasad, M. R.; Young, K. H.; Rodriguiz, R. M.; Wetsel, W. C.; Peters, K. B.; Spasojevic, I.; Herndon II, J. I.; Batinic-Haberle, I.; Dewhirst, M. W. Radioprotection of the brain white matter by Mn(III) N-butoxyethylpyridylporphyrin-based superoxide dismutase mimic, MnTnBuOE-2-PyP5+. *Mol Cancer Ther* **In Revision**; 2014.

[11]   Leu, D.; Zou, Y.; Weitner, T.; Tovmasyan, A.; Spasojevic, I.; Batinic-Haberle, I.; Huang, T.-T. Radiation protection of hippocampal neurogenesis with Mn-containing porphyrins. *The 60th Annual Meeting of the Radiation Research Society* Las Vegas, Nevada, USA; 2014.

[12]   Ashcraft, K. A.; Palmer, G.; Spasojevic, I.; Batinic-Haberle, I.; Dewhirst, M. W. Radioprotection of the salivary gland and oral mucosa with a novel porphyrin-based antioxidant. *58th Annual Meeting of the Radiation Research Society*:**129; 2012.

[13]   Jaramillo, M. C.; Briehl, M. M.; Crapo, J. D.; Batinic-Haberle, I.; Tome, M. E. Manganese porphyrin, MnTE-2-PyP5+, Acts as a pro-oxidant to potentiate glucocorticoid-induced apoptosis in lymphoma cells. *Free Radic Biol Med* **52:**1272-1284; 2012.

[14]   Jaramillo, M. C.; Frye, J. B.; Crapo, J. D.; Briehl, M. M.; Tome, M. E. Increased manganese superoxide dismutase expression or treatment with manganese porphyrin potentiates dexamethasone-induced apoptosis in lymphoma cells. *Cancer Res* **69:**5450-5457; 2009.

---

[15]   Tovmasyan, A.; Weitner, T.; Jaramillo, M.; Wedmann, R.; Roberts, E.; Leong, K. W.; Filipovic, M.; Ivanovic-Burmazovic, I.; Benov, L.; Tome, M.; Batinic-Haberle, I. We have come a long way with Mn porphyrins: from superoxide dismutation to H_2O_2-driven pathways. *Free Rad Biol Med* **65:**S133; 2013.

[16]   Tovmasyan, A.; Weitner, T.; Roberts, E.; Jaramillo, M.; Spasojevic, I.; Leong, K.; Tome, M.; Benov, L.; Batinic-Haberle, I. Understanding differences in mechanisms of action of Fe vs Mn porphyrins: comparison of their reactivities towards cellular reductants and reactive species. *Free Radic Biol Med* **53:**S120; 2012.

[17]   Evans, M. K.; Tovmasyan, A.; Batinic-Haberle, I.; Devi, G. R. Mn porphyrin in combination with ascorbate acts as a pro-oxidant and mediates caspase-independent cancer cell death. *Free Radic Biol Med* **68:**302-314; 2014.

[18]   Ye, X.; Fels, D.; Tovmasyan, A.; Aird, K. M.; Dedeugd, C.; Allensworth, J. L.; Kos, I.; Park, W.; Spasojevic, I.; Devi, G. R.; Dewhirst, M. W.; Leong, K. W.; Batinic-Haberle, I. Cytotoxic effects of Mn(III) N-alkylpyridylporphyrins in the presence of cellular reductant, ascorbate. *Free Radic Res* **45:**1289-1306; 2011.

[19]   Rawal, M.; Schroeder, S. R.; Wagner, B. A.; Cushing, C. M.; Welsh, J. L.; Button, A. M.; Du, J.; Sibenaller, Z. A.; Buettner, G. R.; Cullen, J. J. Manganoporphyrins Increase Ascorbate-Induced Cytotoxicity by Enhancing H2O2 Generation. *Cancer Res* **73:**5232-5241; 2013.

[20]   Oberley-Deegan, R. E.; Steffan, J. J.; Rove, K. O.; Pate, K. M.; Weaver, M. W.; Spasojevic, I.; Frederick, B.; Raben, D.; Meacham, R. B.; Crapo, J. D.; Koul, H. K. The Antioxidant, MnTE-2-PyP, Prevents Side-Effects Incurred by Prostate Cancer Irradiation. *PLoS One* **7:**e44178; 2012.

[21]   Batinic-Haberle, I.; Ndengele, M. M.; Cuzzocrea, S.; Reboucas, J. S.; Spasojevic, I.; Salvemini, D. Lipophilicity is a critical parameter that dominates the efficacy of metalloporphyrins in blocking the development of morphine antinociceptive tolerance through peroxynitrite-mediated pathways. *Free Radic Biol Med* **46:**212-219; 2009.

[22]   Liu, T.; Ji, R. R. Oxidative stress induces itch via activation of transient receptor potential subtype ankyrin 1 in mice. *Neurosci Bull* **28:**145-154; 2012.

[23]   Jumbo-Lucioni, P. P.; Ryan, E. L.; Hopson, M. L.; Bishop, H. M.; Weitner, T.; Tovmasyan, A.; Spasojevic, I.; Batinic-Haberle, I.; Liang, Y.; Jones, D. P.; Fridovich-Keil, J. L. Manganese-Based Superoxide Dismutase Mimics Modify Both Acute and Long-Term Outcome Severity in a Drosophila melanogaster Model of Classic Galactosemia. *Antioxid Redox Signal* **20:**2361-2371; 2014.

[24]   Weitner, T.; Kos, I.; Sheng, H.; Tovmasyan, A.; Reboucas, J. S.; Fan, P.; Warner, D. S.; Vujaskovic, Z.; Batinic-Haberle, I.; Spasojevic, I. Comprehensive pharmacokinetic studies and oral bioavailability of two Mn porphyrin-based SOD mimics, MnTE-2-PyP(5+) and MnTnHex-2-PyP(5+). *Free Radic Biol Med* **58:**73-80; 2013.

[25]   Batinić-Haberle, I.; Spasojević, I.; Stevens, R. D.; Hambright, P.; Fridovich, I. Manganese(III) *meso*-tetrakis(*ortho*-*N*-alkylpyridyl)porphyrins. Synthesis, characterization, and catalysis of $O_2^{\cdot-}$ dismutation. *J. Chem. Soc., Dalton Trans.*:2689-2696; 2002.

[26]   Kos, I.; Reboucas, J. S.; DeFreitas-Silva, G.; Salvemini, D.; Vujaskovic, Z.; Dewhirst, M. W.; Spasojevic, I.; Batinic-Haberle, I. Lipophilicity of potent porphyrin-based antioxidants: comparison of ortho and meta isomers of Mn(III) N-alkylpyridylporphyrins. *Free Radic Biol Med* **47:**72-78; 2009.

[27]   Spasojevic, I.; Menzeleev, R.; White, P. S.; Fridovich, I. Rotational isomers of N-alkylpyridylporphyrins and their metal complexes. HPLC separation, H-1 NMR and X-ray structural characterization, electrochemistry, and catalysis of O-2(center dot-) disproportionation. *Inorganic Chemistry* **41:**5874-5881; 2002.

[28]   Spasojevic, I.; Li, A.; Tovmasyan, A.; Rajic, Z.; Salvemini, D.; St Clair, D.; Valentine, J. S.; Vujaskovic, Z.; Gralla, E. B.; Batinic-Haberle, I. Accumulation of Porphyrin-based SOD Mimics in Mitochondria is Proportional to Their Lipophilicity: S-cerevisiae Study of ortho Mn(III) N-alkylpyridylporphyrins. *Free Radic Biol Med* **49:**S199-S199; 2010.

[29]   Rausaria, S.; Ghaffari, M. M.; Kamadulski, A.; Rodgers, K.; Bryant, L.; Chen, Z.; Doyle, T.; Shaw, M. J.; Salvemini, D.; Neumann, W. L. Retooling manganese(III) porphyrin-based peroxynitrite decomposition catalysts for selectivity and oral activity: a potential new strategy for treating chronic pain. *J Med Chem* **54:**8658-8669; 2011.

[30]   Spasojevic, I.; Chen, Y.; Noel, T. J.; Fan, P.; Zhang, L.; Reboucas, J. S.; St Clair, D. K.; Batinic-Haberle, I. Pharmacokinetics of the potent redox-modulating manganese porphyrin, MnTE-2-PyP(5+), in plasma and major organs of B6C3F1 mice. *Free Radic Biol Med* **45:**943-949; 2008.

[31]   Spasojevic, I.; Chen, Y.; Noel, T. J.; Yu, Y.; Cole, M. P.; Zhang, L.; Zhao, Y.; St Clair, D. K.; Batinic-Haberle, I. Mn porphyrin-based superoxide dismutase (SOD) mimic, MnIIITE-2-PyP5+, targets mouse heart mitochondria. *Free Radic Biol Med* **42:**1193-1200; 2007.

[32]   Spasojevic, I.; Kos, I.; Benov, L. T.; Rajic, Z.; Fels, D.; Dedeugd, C.; Ye, X.; Vujaskovic, Z.; Reboucas, J. S.; Leong, K. W.; Dewhirst, M. W.; Batinic-Haberle, I. Bioavailability of metalloporphyrin-based SOD mimics is greatly influenced by a single charge residing on a Mn site. *Free Radic Res* **45:**188-200; 2011.

[33]   Kos, I.; Benov, L.; Spasojevic, I.; Reboucas, J. S.; Batinic-Haberle, I. High lipophilicity of meta Mn(III) N-alkylpyridylporphyrin-based superoxide dismutase mimics compensates for their lower antioxidant potency and makes them as effective as ortho analogues in protecting superoxide dismutase-deficient Escherichia coli. *J Med Chem* **52:**7868-7872; 2009.

[34]   Miriyala, S.; Thippakorn, C.; Chaiswing, L.; Xu, Y.; Noel, T.; Tovmasyan, A.; Batinic-Haberle, I.; Kooi, C. V.; Chi, W.; Latif, A. A.; Reda, H.; Oberley, T.; Prachayasittikul, V.; Clair, D. K. 4-hydroxy-2-nonenal triggers AIFM2-mediated retrograde signaling by activating its translocation and function switching. *Submitted*; 2013.

[35]   Sheng, H.; Spasojevic, I.; Tse, H. M.; Jung, J. Y.; Hong, J.; Zhang, Z.; Piganelli, J. D.; Batinic-Haberle, I.; Warner, D. S. Neuroprotective Efficacy from a Lipophilic Redox-Modulating Mn(III) N-Hexylpyridylporphyrin, MnTnHex-2-PyP: Rodent Models of Ischemic Stroke and Subarachnoid Hemorrhage. *J Pharmacol Exp Ther* **338:**906-916; 2011.

[36]   Tovmasyan, A. G.; Rajic, Z.; Spasojevic, I.; Reboucas, J. S.; Chen, X.; Salvemini, D.; Sheng, H.; Warner, D. S.; Benov, L.; Batinic-Haberle, I. Methoxy-derivatization of alkyl chains increases the in vivo efficacy of cationic Mn porphyrins. Synthesis, characterization, SOD-like activity, and SOD-deficient E. coli study of meta Mn(III) N-methoxyalkylpyridylporphyrins. *Dalton Trans* **40:**4111-4121; 2011.

[37]   Ezzeddine, R.; Al-Banaw, A.; Tovmasyan, A.; Craik, J. D.; Batinic-Haberle, I.; Benov, L. T. Effect of molecular characteristics on cellular uptake, subcellular localization, and phototoxicity of Zn(II) N-alkylpyridylporphyrins. *J Biol Chem* **288:**36579-36588; 2013.

[38]   Batinic-Haberle, I.; Spasojevic, I.; Tse, H. M.; Tovmasyan, A.; Rajic, Z.; St Clair, D. K.; Vujaskovic, Z.; Dewhirst, M. W.; Piganelli, J. D. Design of Mn porphyrins for treating oxidative stress injuries and their redox-based regulation of cellular transcriptional activities. *Amino Acids* **42:**95-113; 2012.

[39]   Benov, L.; Craik, J.; Batinic-Haberle, I. Protein damage by photo-activated Zn(II) N-alkylpyridylporphyrins. *Amino Acids* **42:**117-128; 2012.

[40]   Ross, A. D.; Sheng, H.; Warner, D. S.; Piantadosi, C. A.; Batinic-Haberle, I.; Day, B. J.; Crapo, J. D. Hemodynamic effects of metalloporphyrin catalytic antioxidants: structure-activity relationships and species specificity. *Free Radic Biol Med* **33:**1657-1669; 2002.

Application of the Rat Grimace Scale to Measure Evoked Pain From Cold Allodynia

Schneider, L.E.[1], Henley, K.Y.[1], and Floyd, C.L.[1]
[1]Department of Physical Medicine and Rehabilitation
University of Alabama at Birmingham, Birmingham, USA

THE UNIVERSITY OF ALABAMA AT BIRMINGHAM
Knowledge that will change your world

UAB CENTER FOR GLIAL BIOLOGY IN MEDICINE
Crossing Boundaries In Neuroscience Research™

Introduction:

Spinal cord injury (SCI) affects 250,000–350,000 people in the US with 12,000 new cases annually (1). One of the most detrimental consequences of SCI is the onset and persistence of SCI-induced neuropathic pain (SCI-NP). Of SCI patients, 60%-80% experience SCI-NP and 1/3 of those describe the pain as debilitating. Understanding the pathobiology of SCI-NP is of great interest to the clinical community and alleviation of SCI-NP is one of the highest priorities for the patient, thus it is critical that animal models correctly emulate the presence of SCI-NP. Many relevant models accomplish this; however questions remain regarding whether an animal's paw withdrawal responses to a stimulus are reflexive (i.e., without supra-spinal involvement) and not indicative of pain. The rat grimace scale (RGS) was developed in acute pain models to measure non-reflexive supra-spinal pain after major surgery or inflammation. In the current study we have developed a method to utilize the RGS to measure supra spinal pain-like responses after SCI. We hypothesize that:

- Rats receiving SCI will exhibit **spontaneous** pain after SCI compared to controls
- Below lesion stimulus in SCI rats will increase **evoked** supra-spinal pain-like responses
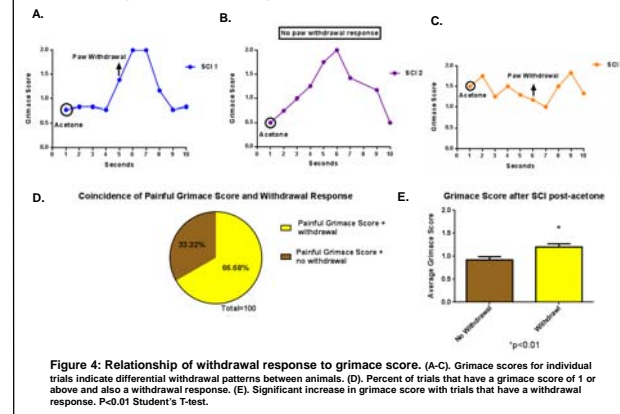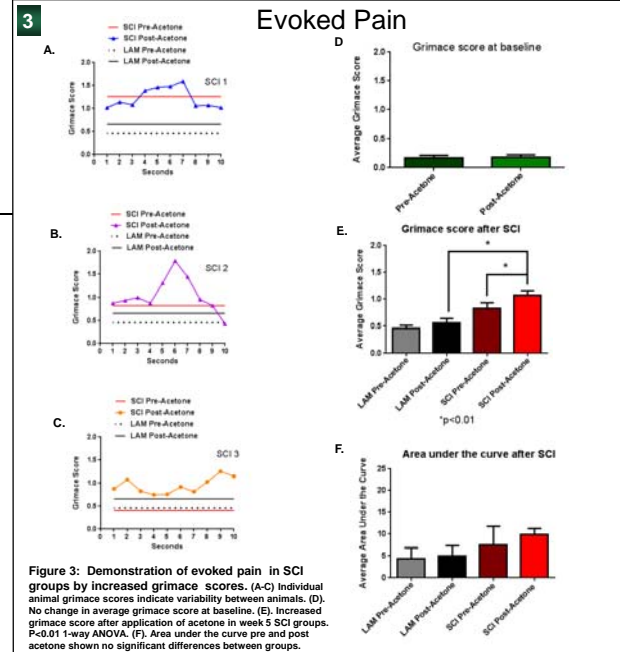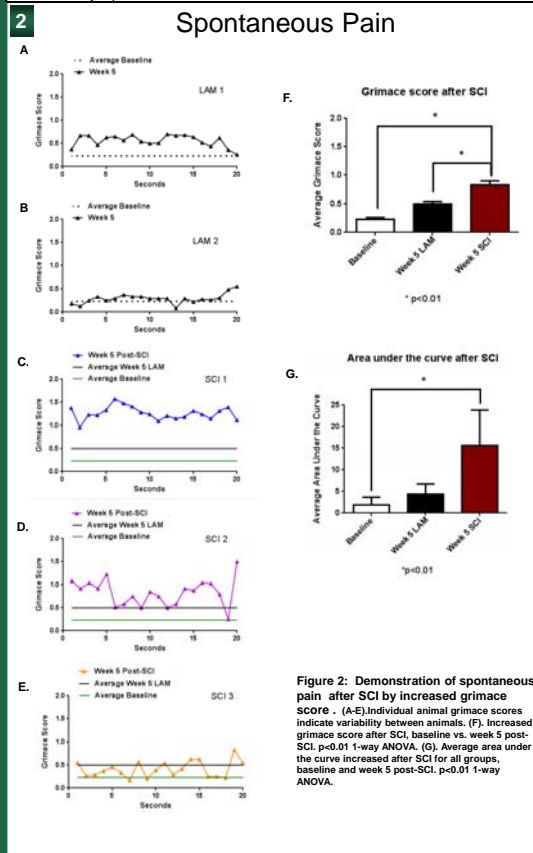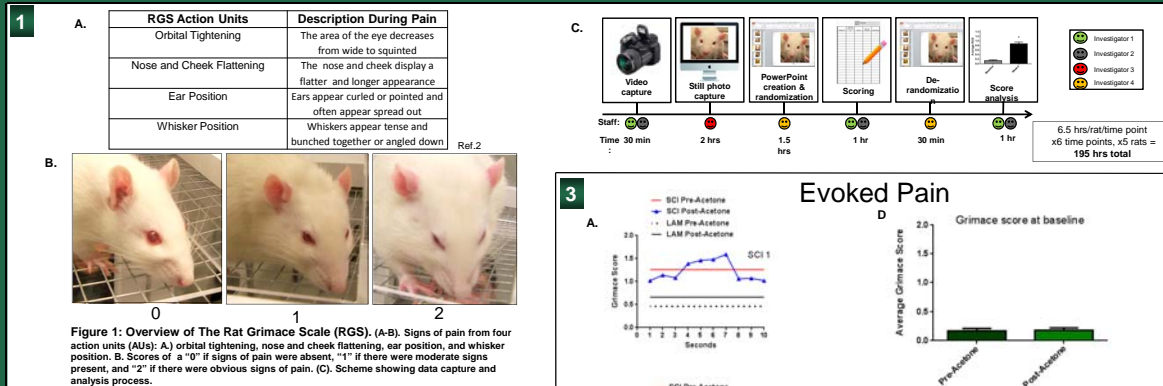
Methods:

Experimental Groups and Injury

- Adult male Sprague-Dawley rats were randomly assigned to one of the following groups: laminectomy (LAM) uninjured controls or spinal cord injured (SCI).
- Hemi-contusion SCI at C5 was induced using the Infinite Horizons impactor with a force of 300kDa.
- Animals were impacted on the side of the spinal cord (hemi-contusion) corresponding to the dominant forepaw, measured at baseline with paw-placement. LAM animals received all surgical procedures except the impact.

Grimace Filming and Application of Acetone

- Testing occurred one week prior to SCI (baseline) and continued once per week for 6 weeks after SCI.
- Rats were placed in a clear Plexiglas box (20cm x 9cm x 10cm) on an elevated platform with a wire mesh bottom. The animal's face (including nose/cheek, whiskers, eyes, and ears) was actively filmed for one minute prior to stimulus. This represents the "before" acetone period.
- A drop of acetone was applied using a syringe to the plantar surface of the contralateral hind limb. The face was filmed for 1 minute, representing the "after" acetone period. Hind paw withdraw responses were recorded within 20 seconds after the application of the acetone.
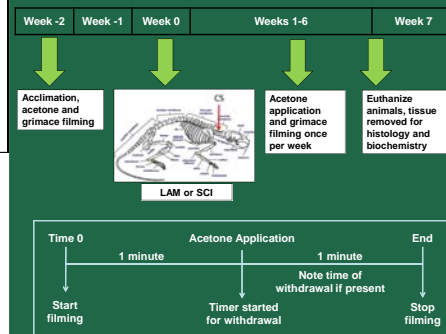
Data Capture and Analysis

- One screen shot was taken from the video each second for the 20 seconds prior to and 20 seconds after the application of acetone. The screen shots for all three tests were combined into a PowerPoint presentation, given a unique coding number, and randomized using a Power Point macro code (Fig 1c.)
- The PowerPoint slides of the animal's face was scored by raters naïve to the condition using the Rat Grimace Scale (2) (RGS) Fig.1.
- The average score for each action unit was calculated for each slide. Slide scores were then averaged across 2 raters and split into "before" acetone and "after" acetone.

Results:

1

A.

RGS Action Units	Description During Pain
Orbital Tightening	The area of the eye decreases from wide to squinted
Nose and Cheek Flattening	The nose and cheek display a flatter and longer appearance
Ear Position	Ears appear curled or pointed and often appear spread out
Whisker Position	Whiskers appear tense and bunched together or angled down

Ref.2

B.
0   1   2

C.
Video capture — Still photo capture — PowerPoint creation & randomization — Scoring — De-randomizatio — Score analysis

Investigator 1, Investigator 2, Investigator 3, Investigator 4

Staff: Time 30 min, 2 hrs, 1.5 hrs, 1 hr, 30 min, 1 hr
6.5 hrs/rat/time point x6 time points, x5 rats = 195 hrs total

Figure 1: Overview of The Rat Grimace Scale (RGS). (A-B). Signs of pain from four action units (AUs): A.) orbital tightening, nose and cheek flattening, ear position, and whisker position. B. Scores of a "0" if signs of pain were absent, "1" if there were moderate signs present, and "2" if there were obvious signs of pain. (C). Scheme showing data capture and analysis process.

2 Spontaneous Pain

A. LAM 1
B. LAM 2
C. SCI 1
D. SCI 2
E. SCI 3

F. Grimace score after SCI
* p<0.01

G. Area under the curve after SCI
* p<0.01

Figure 2: Demonstration of spontaneous pain after SCI by increased grimace score. (A-E).Individual animal grimace scores indicate variability between animals. (F). Increased grimace score after SCI, baseline vs. week 5 post-SCI. p<0.01 1-way ANOVA. (G). Average area under the curve increased after SCI for all groups, baseline and week 5 post-SCI. p<0.01 1-way ANOVA.

3 Evoked Pain

A. SCI 1
B. SCI 2
C. SCI 3

D. Grimace score at baseline
E. Grimace score after SCI * p<0.01
F. Area under the curve after SCI

Figure 3: Demonstration of evoked pain in SCI groups by increased grimace scores. (A-C) Individual animal grimace scores indicate variability between animals. (D). No change in average grimace score at baseline. (E). Increased grimace score after application of acetone in week 5 SCI groups. P<0.01 1-way ANOVA. (F). Area under the curve pre and post acetone shown no significant differences between groups.

A. SCI 1
B. No paw withdrawal response SCI 2
C. SCI 3

D. Coincidence of Painful Grimace Score and Withdrawal Response
Painful Grimace Score + withdrawal
Painful Grimace Score + no withdrawal
33.32%
66.68%
Total=100

E. Grimace Score after SCI post-acetone *p<0.01
No withdrawal / withdrawal

Figure 4: Relationship of withdrawal response to grimace score. (A-C). Grimace scores for individual trials indicate differential withdrawal patterns between animals. (D). Percent of trials that have a grimace score of 1 or above and also a withdrawal response. (E). Significant increase in grimace score with trials that have a withdrawal response. P<0.01 Student's T-test.

Summary of Methods:

Week -2	Week -1	Week 0	Weeks 1-6	Week 7
Acclimation, acetone and grimace filming		Acetone application and grimace filming	Acetone application and grimace filming once per week	Euthanize animals, tissue removed for histology and biochemistry

LAM or SCI

Time 0 — Acetone Application — End
1 minute — 1 minute
Start filming — Timer started for withdrawal — Note time of withdrawal if present — Stop filming

Summary of Results:

- There is an overall increase in grimace score as a result of SCI.
- Animals have different levels of spontaneous pain detectable by the RGS.
- There is an overall increase in grimace score with application of acetone after SCI (evoked response).
- Animals have different levels of evoked pain in response to acetone that is detectable by the RGS.
- There is an increased grimace score associated with withdrawal response ~2/3 of the time. Thus the reflexive withdrawal is not always an indicator of pain.

Future Directions:

- Utilize the RGS to characterize the variability of spontaneous pain in this and other animal models of SCI.
- Utilize the RGS to test the efficacy of analgesic therapeutic strategies.
- Elucidate the relationship between spontaneous and evoked pain after SCI.

References:

1. *The 2010 Annual Statistical Report for the Spinal Cord Injury Model Systems.* National Spinal Cord Injury Statistical Center 2010 [cited 2010; Available from: http://www.uab.edu/medicine/sci.

2. Susana G. Sotocinal, Robert E. Sorge, Austin Zaloum, Alexander H Tuttle, Loren J. Martin, Jeffery S. Wieskopf, Josiane CS. Mapplebeck, Peng Wei, Shu Zhan, Shuren Zhang, Jason J McDougall, Oliver D. King and Jeffery S. Mogil. The Rat Grimace Scale: A partially automated method for quantifying pain in the laboratory rat via facial expressions. Molecular Pain 2011, 7:55.

Acknowledgements: